ANL/CEN/FE-79-5

SUPPORT STUDIES IN FLUIDIZED-BED COMBUSTION

Quarterly Report
January—March 1979

by

Irving Johnson, S. H. D. Lee, J. A. Shearer,
E. B. Smyk, W. M. Swift, F. G. Teats,
C. B. Turner, W. I. Wilson, and A. A. Jonke

U of C-AUA-USDOE

ARGONNE NATIONAL LABORATORY, ARGONNE, ILLINOIS

Prepared for the U. S. DEPARTMENT OF ENERGY
under Contract W-31-109-Eng-38

DISCLAIMER

Printed in the United States of America
Available from
National Technical Information Service
U. S. Department of Commerce
5285 Port Royal Road
Springfield, VA 22161

NTIS price codes
Printed copy: A04
Microfiche copy: A01

Distribution Category:
Coal Conversion and Utilization--
Direct Combustion of Coal
(UC-90e)

ANL/CEN/FE-79-5

ARGONNE NATIONAL LABORATORY
9700 South Cass Avenue
Argonne, Illinois 60439

SUPPORT STUDIES IN FLUIDIZED-BED COMBUSTION

Quarterly Report
January—March 1979

by

Irving Johnson, S. H. D. Lee, J. A. Shearer,
E. B. Smyk, W. M. Swift, F. G. Teats, C. B. Turner,
W. I. Wilson, and A. A. Jonke

Chemical Engineering Division

Prepared for the
U. S. Department of Energy
under Contract No. W-31-109-Eng-38
and the
U. S. Environmental Protection Agency
under Agreement IAG-D5-E681

Previous reports in this series

ANL/CEN/FE-78-3
ANL/CEN/FE-78-4
ANL/CEN/FE-78-10
ANL/CEN/FE-79-3

BIBLIOGRAPHIC DATA SHEET	1. Report No. ANL/CEN/FE-79-5	2.	3. Recipient's Accession No.
4. Title and Subtitle Support Studies in Fluidized-Bed Combustion, Quarterly Report, January-March 1979			5. Report Date May 1979 6.
7. Author(s) I. Johnson, S. H. D. Lee, J. A. Shearer, E. B. Smyk, W. M. Swift, F. G. Teats, C. B. Turner, W. I. Wilson, A. A. Jonke			8. Performing Organization Rept. No. ANL/CEN/FE-79-5
9. Performing Organization Name and Address Argonne National Laboratory 9700 South Cass Avenue Argonne, Illinois 60439			10. Project/Task/Work Unit No. 11. Contract/Grant No. W31-109-ENG-38 (DOE) IAG-D5-E681 (EPA)
12. Sponsoring Organization Name and Address U. S. Department of Energy and the U. S. Environmental Protection Agency			13. Type of Report & Period Covered Quarterly January-March 1979 14.

15. Supplementary Notes

16. Abstracts

This work supports the development studies for atmospheric and pressurized fluidized-bed coal combustion. Laboratory and process development studies are aimed at providing needed information on limestone utilization, control of emission of alkali metal compounds and SO_2, particulate loadings of flue gas, and other aspects of fluidized-bed coal combustion.

This report presents information on: the removal of gaseous alkali metal compounds from hot flue gas using granular sorbents, results of tests of the efficiency of a commercial high-efficiency cyclone (TAN-JET), information on particulate emissions from FBCs, and the effect of $CaCl_2$ and Na_2CO_3 on the sulfation of limestone.

17. Key Words and Document Analysis. 17a. Descriptors

Additives	Combustion	Fossil Fuels
Air Pollution	Cyclone Separators	Limestone
Bauxite	Diatomaceous Earth	Particle Size
Calcium Chloride	Dolomite	Porosity
Calcium Oxides	Flue Gas	Sodium Carbonate
Calcium Sulfates	Fluidized-Bed Combustion	Sodium Chlorides
Coal	Fly Ash Leaching	Sulfur Oxides

17b. Identifiers/Open-Ended Terms

Activated Bauxite
Granular Bed Filter
Sorbent Enhancement
Sorbent Regeneration
Sorbent Sulfation
Stone Morphology

17c. COSATI Field/Group 13 B

18. Availability Statement	19. Security Class (This Report) UNCLASSIFIED	21. No. of Pages
	20. Security Class (This Page UNCLASSIFIED	22. Price

TABLE OF CONTENTS

LIST OF FIGURES

LIST OF FIGURES (contd)

LIST OF TABLES

SUPPORT STUDIES IN FLUIDIZED-BED COMBUSTION

Quarterly Report
January—March 1979

by

Irving Johnson, S. H. D. Lee, J. A. Shearer,
E. B. Smyk, W. M. Swift, F. G. Teats, C. B. Turner,
W. I. Wilson, and A. A. Jonke

ABSTRACT

This work supports the development studies for atmospheric and pressurized fluidized-bed coal combustion. Laboratory and process development studies are aimed at providing needed information on limestone utilization, control of emission of alkali metal compounds and SO_2, particulate loadings of flue gas, and other aspects of fluidized-bed coal combustion.

This report presents information on: the removal of gaseous alkali metal compounds from hot flue gas using granular sorbents, results of tests of the efficiency of a commercial high-efficiency cyclone (TAN-JET), information on particulate emissions from FBCs, and the effect of $CaCl_2$ and Na_2CO_3 on the sulfation of limestone.

SUMMARY

Task A. Hot Gas Cleanup

Removal of Alkali Metal Compounds from Hot Flue Gas of Coal Combustion. In the potential application of pressurized fluidized-bed combustion of coal for power generation, corrosion of blades of associated gas turbines due to alkali metal compounds present in the flue gas may be a problem. The objective of this task is to develop an effective sorbent for use in a hot fixed-bed filter to remove alkali metal compounds from a hot flue gas.

Diatomaceous earth and activated bauxite have been found to be very effective sorbents. The effects of sorbent bed temperature, superficial gas velocity, and gas hourly space velocity on sorbent reactivity are reported. Presented are the results of additional experiments (1) to measure the effect of NaCl-vapor concentration in the flue gas on the sorption efficiency of diatomaceous earth and (2) to determine the regenerability of activated bauxite for NaCl vapor capture.

At gas hourly space velocities of 18,600 and 33,500 h^{-1}, the average rate of NaCl vapor sorption by diatomaceous earth increases as a linear function of increasing NaCl vapor concentration. As expected, however, the efficiency, in terms of percent NaCl vapor captured by the sorbent in a fixed bed,

decreases with increased experiment duration. Lower NaCl vapor concentrations, lower gas velocities, and longer contact times of the flue gas and diatomaceous earth result in substantially increased removal efficiency.

To investigate the effect of regeneration on the sorption performance of activated bauxite, ten cycles of NaCl-vapor sorption and water-leaching regeneration experiments have been performed. It was found that over the ten cycles, the reactivity of the sorbent for NaCl vapor capture remained unaffected by regeneration. Removal efficiency was between 95 and 98%. Attrition losses were low, averaging only 2% per cycle.

Particle Removal from Flue Gas. In PFBC, the hot flue gas from the combustor must be expanded through a gas turbine to recover energy. To protect the turbine from damage, the particle mass loading must be reduced to acceptably low levels. Reported are the results of testing a high-efficiency cyclone for particulate removal in the flue gas system of ANL's 15.2-cm-dia pressurized fluidized-bed combustor. Presented are (1) an analysis of data on the effect on cyclone efficiency of pressure drop at the secondary air inlet nozzle, (2) the results of experiments measuring cyclone efficiency at 810-kPa system pressure, and (3) the results of an attempt to determine TAN-JET size selectivity.

The results of experiments measuring cyclone efficiency at ambient and 300-kPa system pressure were correlated, using a power curve least squares fit of the data. The data were correlated against the mass loading in the flue gas entering the cyclone at three different levels of pressure drop across the secondary air inlet nozzle. Loadings in the flue gas leaving the TAN-JET when operating at a nozzle pressure drop of 105 kPa or 140 kPa and with an inlet loading of 2.5 to 3.5 g/m^3 were on the order of 0.15 g/m^3.

During experiments measuring cyclone performance at 810-kPa system pressure, problems of gas leakage from the cyclone pressure shell and of solids plugging the cyclone ash discharge line were encountered. After steps were taken to correct these problems, additional experiments at 810-kPa system pressure resulted in erratic results which were inconsistent with the correlations of the low-pressure data. A new ash receiver vessel is being fabricated to permit modification of the ash discharge line in an attempt to improve the high-pressure performance of the cyclone.

Samples of fly ash recovered from the TAN-JET ash receiver and from a sintered metal filter downstream from the cyclone were split into fractions and analyzed for size distribution at two independent laboratories, using Coulter counters. The discrepancies between the distributions reported for the samples were very large (about one order of magnitude in mass mean diameter). As a matter of interest, the two separate sets of size distribution data were used to generate size selectivity curves for the TAN-JET cyclone. One set of data indicated a cut diameter for the cyclone of 0.9 μm, well below the theoretical cut diameter of 2.1 μm. The other set of data gave an estimated cut diameter of 5.9 μm.

Task B. Trace Pollutants

Assessment of Particulate Emissions from Atmospheric Fluidized-Bed Combustors. The state of knowledge of particulate emissions from AFBCs has been assessed. Information was obtained on the effects of various parameters on dust loading, particle size distribution, and chemical composition. Since the results reported vary over broad ranges and since most of the results were not obtained in large units, much more work needs to be done before a particulate emission control system could be designed for an AFBC with any degree of confidence.

Task C. Limestone Utilization

Enhancement of Limestone Sulfation. To decrease the amount of limestone needed for the control of SO_2 emission levels in the off-gas from fluidized-bed combustion systems, various salts are being investigated as sulfation enhancement agents. It has been found that these sulfation enhancement agents operate by means of the effect that they produce on the porosity of the calcined limestone. Larger pores have been observed in a limestone calcined (i.e., converted from $CaCO_3$ to CaO) while various salts (e.g., NaCl and $CaCl_2$) were in contact with the limestone than in stones calcined without salts present. These large pores permit gaseous SO_2 to penetrate deep into the limestone particle and to react and form $CaSO_4$. Where pores are small, $CaSO_4$ that forms rapidly at the mouths of pores plugs them and hinders the penetration of gas into the interior of limestone particles.

In this report, scanning electron microphotographs (SEMs) of the surface and interior of calcined limestones which had been treated with various amounts of $CaCl_2$ are shown. The remarkable effect of the $CaCl_2$ on the grain size and the porosity of the calcined stones is clearly seen in these SEMs.

Other SEMs show particles from a sample of limestone which was first sulfated with no salt present and then treated with NaCl and reheated. Sulfur scans of particles from the initial sulfation showed sulfur confined to the surface; after salt treatment and heating, sulfur was distributed throughout the particle. These results help explain earlier observations that addition of salt to a FBC bed of spent limestone (which had ceased to sorb SO_2) reactivates SO_2 removal.

Most studies have been done with calcitic limestones. However, the addition of salts to dolomitic limestones also can increase SO_2 reactivity. The effects of $CaCl_2$ additions (between 0.1 and 5 mol %) are reported for nine different dolomitic limestones whose extent of reaction (when not treated with $CaCl_2$) varies from 18 to 92%. The addition of 0.1 mol % $CaCl_2$ had a significant effect on increasing sulfation for all stones. As the amount of $CaCl_2$ added was further increased, the effect on sulfation decreased until there was a minimum effect at 0.5 to 1 mol % $CaCl_2$. Then, addition of larger amounts of $CaCl_2$ caused the extent of sulfation to increase. The latter results, which are similar to those observed with $CaCl_2$ for calcitic limestone, can be explained as due to the postulated formation of a liquid $CaCl_2$-CaO solution

which is very reactive with gaseous SO_2. SEMs show the large effects of $CaCl_2$ treatment on the porosity of calcined dolomites.

Preliminary data are reported which show that Na_2CO_3 is very effective in enhancing the sulfation of limestones. This enhancement agent is under study since it is believed to be less corrosive than NaCl.

The effect of temperature (over the range 750-1050°C) on the extent of sulfation possible for a calcitic limestone was measured, using a laboratory TGA. Results are given for virgin stone and for stone treated with 1% NaCl and 0.1% $CaCl_2$. For the untreated stone, the extent of sulfation decreased as the temperature was increased. For the salt-treated stones, the extent of sulfation passed through a minimum as the temperature was increased.High conversions were obtained at high temperatures. If the same results are obtained in an actual FBC, alternative salts may permit the operating temperature to be increased. This would be expected to lead to higher combustion efficiencies.

TASK A. HOT GAS CLEANUP

1. Removal of Alkali Metal Compounds from Hot Flue Gas of Coal Combustion (S. H. D. Lee and W. A. Boyd)

In the prospective application of pressurized fluidized-bed combustion of coal to power generation, the corrosion of turbine blades in a gas turbine due to the attack of alkali metal compounds in the hot flue gas from the combustor appears to be a potential problem. This problem can be eliminated by reducing the concentration of alkali metal compounds in the hot flue gas to a level tolerable for a turbine blade. A way to accomplish this is to use a hot fixed-bed filter containing a sorbent that removes the alkali metal compounds from the hot flue gas before the gas is expanded into a turbine.

The objective of this task is to develop an effective sorbent as bed material for the filter. Several types of materials have been tested as candidate sorbents in this work. Among them, diatomaceous earth and activated bauxite were found to be the most effective sorbents. Studies have been continued to obtain the technical data base needed for the design of granular sorbent fixed-bed filters in which either diatomaceous earth or activated bauxite as sorbent would remove gaseous alkali metal compounds from hot flue gas. The effects of sorbent bed temperature, superficial gas velocity, and gas hourly space velocity of flue gas were studied, and the results were presented in an earlier report of this series, ANL/CEN/FE-78-10. In a continuation of the work performed during the previous quarter, the effect of NaCl vapor concentration in flue gas on the sorption efficiency of diatomaceous earth and the effect of the regenerability of activated bauxite on the sorption performance of NaCl vapor as a function of the sorption-regeneration cycle were established. The sorption tests for all of these studies were carried out using the laboratory-scale, batch-unit combustor system.* The details of this system have been described (ANL/ES-CEN-1016). Sorbents were tested at 800°C and atmospheric pressure using a simulated dry flue gas of PFBC. The flue gas has a volumetric composition of 3% O_2, 16% CO_2, about 300 ppm SO_2, about 180 ppm H_2O, various amounts of NaCl vapor, and the balance N_2. The superficial gas velocity of flue gas passing through the sorbent bed was 66 cm/s, and the particle size of the sorbents tested was -8 +10 mesh.

a. Effects of NaCl Vapor Concentration in Flue Gas, Experiment Duration, and Gas Velocity on the Sorption Efficiency of Diatomaceous Earth

Some results of this series of studies were reported in the previous report of this series (ANL/CEN/FE-79-3). To allow comparison of the earlier and new results, the earlier results are also included in this section. For this series of studies, NaCl vapor sorption by diatomaceous earth was tested as a function of experiment duration, NaCl vapor concentration in the simulated

---

*The combustion system consists of a horizontal tube furnace and associated gas feed lines and product gas analysis instrumentation. The first sector of the tube furnace is a gas preheater; the next sector contains a sample pan which can be heated along with its salt contents; next is a packed granular bed sorbent filter, followed by cold traps and a backup glass wool filter.

flue gas, and gas hourly space velocity (GHSV) of the gas. The distributions of NaCl obtained from this series of tests are tabulated in Table 1, and the results are further plotted in Figs. 1 and 2. Figure 1 is a plot of the

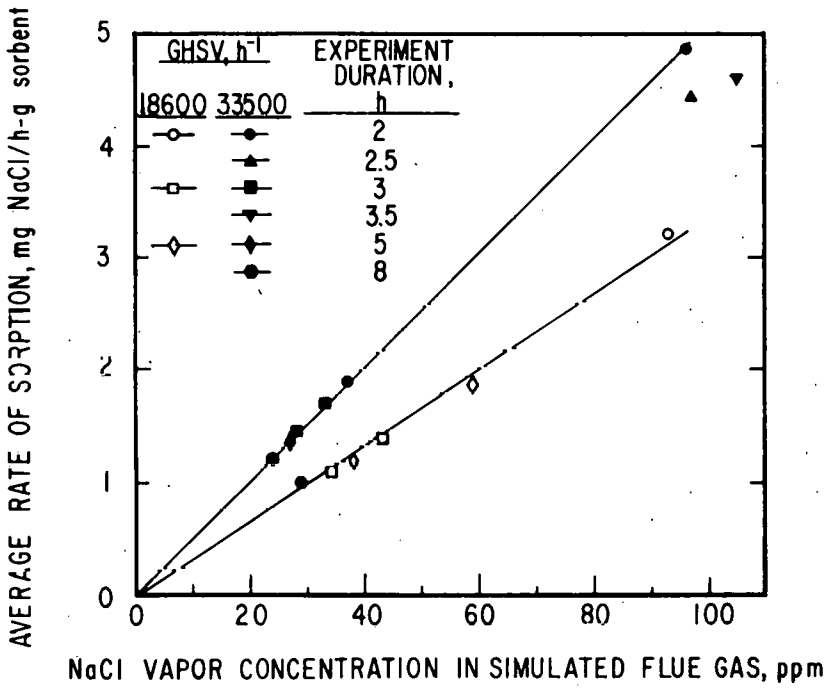

Fig. 1. Average Rate of NaCl Sorption of Diatomaceous Earth as a Function of NaCl Concentration in Flue Gas

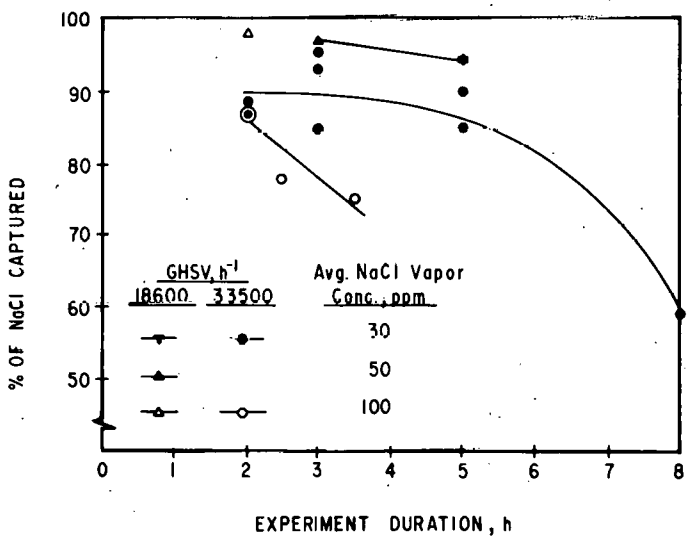

Fig. 2. Effect of NaCl Concentration in Flue Gas on NaCl Capture of Diatomaceous Earth as a Function of Experimental Duration

Table 1. Distribution of NaCl from Testing Diatomaceous Earth (-8 + 10 mesh) for NaCl Vapor Capture as a Function of Experimental Duration, NaCl Concentration in the Flue Gas, and Gas Hourly Space Velocity

The sorbent was tested at 800°C and atmospheric pressure in a simulated flue gas of PFBC at a linear gas velocity of 66 cm/s.

	Experiment HGC-														
	47	66	65	57	57R	58	58R	56	62	55	52R	68	67	75	74
Experiment Duration, h	2	2.5	3.5	2	2	3	3	5	5	8	2	3	5	3	5
Avg NaCl Conc. in Flue Gas, ppm	96	97	105	37	24	33	28	27	27	29	93	43	59	34	38
Quantity of Sorbent, g	30	30	30	13	13	13	13	13	13	13	50	22	22	22	22
GHSV, h^{-1}	← 33500 →										← 18600 →				
	NaCl, mg														
(1) NaCl Collected by															
(a) Cold Trap	29	58	100	5	3	4	7	7	11	51	6	3	11	3	7
(b) Glass-wool Filter	18	37	65	2	2	1	3	3	5	22	4	1	4	1	2
(2) NaCl Captured by Sorbent[a]	292	334	483	49	31	66	57	90	89	104	318	93	206	73	132
(3) Total	339	429	648	56	36	71	67	100	105	177	328	97	221	77	141
(4) Rate of Sorption, mg NaCl/h-g sorbent	4.9	4.4	4.6	1.9	1.2	1.7	1.5	1.4	1.4	1.0	3.2	1.4	1.9	1.1	1.2
(5) % of NaCl Vapor Captured, [(2)/(3)] x 100	86.1	77.9	74.5	87.5	86.1	93.0	85.1	90	84.8	58.8	97.0	95.9	93.2	94.8	93.6

[a]NaCl concentration of the sorbent was measured by dissolving representative samples of the sorbent in a mixture of H_2SO_4, HF, and HNO_3 and then analyzing the solution, using flame emission spectrometry (FE). FE analysis was done by R. W. Bane.

average rate of NaCl vapor sorption by diatomaceous earth as a function of NaCl concentration in the flue gas. In Fig. 2, the percentage of the NaCl vapor captured is plotted as a function of experiment duration.

As shown in Fig. 1, for both of the gas hourly space velocities used (GHSVs of 18600 and 33500 h^{-1}), the average rate of NaCl vapor sorption by diatomaceous earth is a linear function of NaCl vapor concentration. This indicates that the utilization of diatomaceous earth (in terms of the amount of NaCl captured per unit weight of sorbent) decreases with decreasing NaCl concentration in the flue gas. It is also noted that for NaCl vapor concentrations lower than 60 ppm, this linear relationship holds up to an experiment duration of 5 h; however, when NaCl concentration exceeds about 90 ppm, this linear relationship collapses after the first 2 h.

Of practical importance in the development of a sorbent is the effectiveness of the sorbent in removing alkali metal compounds from flue gas. The effect of NaCl concentration in the flue gas on the sorption efficiency of diatomaceous earth is shown in Fig. 2. As expected, the efficiencies (in terms of percent of the NaCl vapor captured by diatomaceous earth) decrease with experiment duration. When NaCl concentration in the flue gas is high, the efficiency is noted to drop sharply with experiment duration; however, when NaCl concentration is lower, the efficiencies remain at significantly higher levels for longer periods of time than at high NaCl concentrations. Fig. 2 also shows that for a given experimental duration, when gas hourly space velocity is reduced (i.e., when the contact time of the flue gas and diatomaceous earth bed is increased), the efficiency is substantially increased. Furthermore, the sorption efficiency is not reduced by reducing the NaCl concentration in the flue gas.

Results from this series of experiments indicate that the utilization of diatomaceous earth (in terms of quantity of NaCl captured per unit weight of sorbent) decreases with decreasing NaCl concentration in the flue gas; however, the efficiency of NaCl vapor removal from flue gas is not reduced due to the reduction of NaCl concentration in the flue gas. The efficiency remains at a higher level for longer periods of experimental duration at low NaCl concentrations than at high NaCl concentrations.

b. NaCl Sorption and Water-Leaching Regeneration of Activated Bauxite

Not only is activated bauxite effective for capturing alkali metal compound vapors (such as NaCl, KCl, and K_2SO_4), but also, it can be easily regenerated by a simple water-leaching process. Its regenerability has been experimentally demonstrated in three cycles of NaCl-sorption and water-leaching regeneration experiments (ANL/CEN/FE-79-3); however, the sorption performance of alkali vapors as a function of the sorption-regeneration cycle is yet to be studied. To investigate that effect, ten cycles of NaCl-vapor sorption and water-leaching regeneration experiments for activated bauxite were performed. The experimental procedures for this set of experiments are shown in the flow sheet in Fig. 3. Results are presented and discussed in this section.

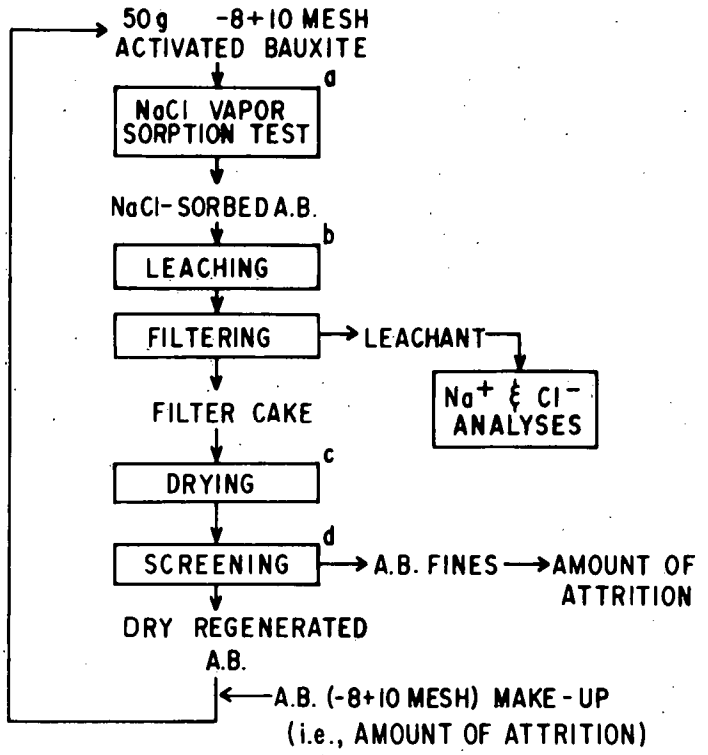

Fig. 3. Flow Sheet of NaCl-Sorption Step and Water-Leaching Regeneration Step for Activated Bauxite (AB)

a. Sorption Test Conditions: 800°C at atmospheric pressure in a simulated dry flue gas of PFBC containing 3% O_2, 16% CO_2, 300 ppm SO_2, about 180 ppm H_2O, about 37 ppm NaCl vapor, and the balance N_2; superficial gas velocity = 66 cm/s; GHSV = 18600 h^{-1} (or contact time of 0.2 s); experiment duration = 5 h.

b. Leaching Conditions: leached with distilled water at gently boiling temperature (about 95°C) for 30 min; for fifth and sixth cycles, the sorbent was first washed with cold distilled water and filtered and then was leached.

c. Drying Conditions: 400°C for 1 h in an air flow.

d. Sieved with 10-mesh screen to discard fines.

In the following discussions, the first cycle of sorption and regeneration represents the fresh activated bauxite; the second cycle represents the regenerated activated bauxite from the first cycle, and so on.

Attrition of Activated Bauxite. During experimental handling and water-leaching regeneration, some activated bauxite fines were produced due to attrition of samples. The amount of attrition not only indicates the rigidity of a sample but also, more importantly, allows estimation of the sample loss during handling and water-leaching regeneration of the sample. Since 50 g of activated bauxite is used for each sorption test, the amount of attrition represents the amount of fresh activated bauxite makeup. Table 2 shows the attrition, in percent, of activated bauxite for the complete ten cycles of tests.

As shown in Table 2, the average attrition was 2%; therefore, except in the first cycle, the amount of fresh activated bauxite added in each cycle for making up the loss as fines was only 2% of the total amount of regenerated activated activated bauxite (50 g).

Table 2. Attrition of Activated Bauxite in Cyclic NaCl-Sorption and Water-Leaching Regeneration

Cycle of Sorption and Regeneration	Wt of AB in Test Bed,[a] g	Wt of Regenerated AB,[b] g	Wt of AB Lost, g	Attrition, %
1	50.00	48.01	1.99	4.0
2	50.00	48.53	1.47	2.9
3	50.00	48.83	1.17	2.3
4	50.00	48.80	1.20	2.4
5	50.00	49.31	0.69	1.4
6	50.00	49.53	0.47	0.9
7	50.00	49.07	0.93	1.9
8	50.00	49.24	0.76	1.5
9	50.00	49.31	0.69	1.4
10	50.00	49.61	0.39	0.8
			Avg	2.0

[a] Wt of activated bauxite used in the bed for NaCl-sorption test.

[b] Wt of -8 +10 mesh regenerated activated bauxite at the end of a cycle.

NaCl Vapor Sorption Performance. The sorbent was tested at a GHSV of simulated flue gas of 18,600 h^{-1}; this GHSV gives a contact time of about 0.2 s between the flue gas and the sorbent bed. All sorption tests were carried out for 5 h. Table 3 shows the results from testing for NaCl vapor capture both fresh activated bauxite and activated bauxite regenerated by water-leaching. The results of experiment HGC-71 were obtained previously from a separate test at the same conditions as in the ten-cycle test.

Table 3. Distributions of NaCl from Testing for NaCl Vapor Capture Fresh Activated Bauxite and Activated Bauxite Regenerated by Water Leaching

Sorbent was tested at 800°C and atmospheric pessure in a simulated dry gas of PFBC at a linear velocity of 66 cm/s and a GHSV of 18600 h^{-1} (or a contact time of 0.2 s). Experiment duration was 5 h.

	Experiment HGC-											
	71	LR1	LR2	LR3	LR4	LR5	LR6	LR7	LR8	LR9	LR10	Avg
Cycle of Sorption and Regeneration	1	1	2	3	4	5	6	7	8	9	10	
Avg NaCl Vapor Conc. in Flue Gas, ppmv	37	43	40	38	35	35	38	35	36	36	35	37
	NaCl, mg											
(1) NaCl Collected on Cold Traps and Glass-Wool Filter	3	2	2	3	3	7	5	2	2	2	3	3
(2) NaCl Captured by Sorbent[a]	136[b]	151	147	138	128	123	136	130	132	132	127	135
(3) Total	139	153	149	141	131	130	141	132	134	134	130	138
(4) % NaCl Captured by Sorbent - [(2)/(3) x 100]	97.8	98.8	98.7	97.9	97.7	94.6	96.5	98.5	98.5	98.5	97.7	97.8

[a]Except for experiment HGC-71, the difference between total NaCl vapor transported to the sorbent bed and item (1).

[b]Obtained by chemical analysis of the sodium content of the sorbent.

As shown in Table 3, the sorbent was tested in a simulated dry flue gas of PFBC containing, on the average, 37 volumetric parts per million (ppmv) NaCl vapor, and the sorbents, both fresh and regenerated, very effectively captured about 98% of the NaCl vapor in the flue gas for the first four cycles (row 4 in Table 3). The efficiency suddenly dropped to 94.6% in the fifth cycle; however, the efficiencies in the rest of the cycles were back up at about 98% again. The sudden drop in efficiency in the fifth cycle was probably due to contamination of the cold traps on which the NaCl vapor that had passed through the sorbent bed was condensed. On the average, the removal efficiency was about 98% for all ten cycles. As noted above, the amount of make-up of fresh activated bauxite added to the regenerated activated bauxite represented only 2% by weight of the total amount of the sorbent (50 g). The removal efficiencies observed for the regenerated activated bauxites were constantly very high, as for fresh activated bauxite, indicating that regenerated activated bauxite is just as effective as fresh activated bauxite.

From results of this series of tests it is concluded that activated bauxite can be effectively regenerated by a simple water-leaching process and that the NaCl vapor removal efficiency of regenerated activated bauxite is not affected by the number of sorption-regeneration cycles.

Water Leachant. All water leachant from water-leaching regeneration was collected for Na^+ and Cl^- analyses. These analyses were intended to double-check the earlier finding that leachable NaCl is retained by activated bauxite by an adsorption process. Tables 4 and 5 show, respectively, the quantities of Na^+ and Cl^- in the leachants of all ten cycles and the total amount of leachable NaCl captured by activated bauxite for each of the complete ten cycles.

Within the limits of analytical and experimental errors, the mole ratio of Na^+ and Cl^- for leachants from all ten cycles is unity on the average (Table 4). These results confirm that the leachable NaCl had been "adsorbed" by activated bauxite. As for the proportion of NaCl captured that was leachable, Table 5 clearly shows that 54% of the NaCl vapor captured by fresh activated bauxite was leachable. The 46% not leachable is believed to have been tied up by clay impurities in activated bauxite. On the average, about 82% of the total NaCl vapor captured by regenerated activated bauxite was leachable. This information indicates that NaCl vapor is captured by regenerated activated bauxite mainly by an adsorption process. An adsorption process is a reversible process--that is, an adsorbent can repeatedly adsorb after desorption of the adsorbate, therefore, regenerated activated bauxite is as effective as fresh activated bauxite (as demonstrated previously).

Both diatomaceous earth and activated bauxite sorbents are being developed for application to the pressurized fluidized-bed combustion of coal. So far, the sorbents were tested only at atmospheric pressure. Theory indicates that increasing the system pressure will increase the sorption efficiency of the sorbent.

Table 4. Sodium and Chloride Ions in the Water Leachants from Regeneration of NaCl-Sorbed Activated Bauxite

NaCl-sorbed activated bauxite was leached with distilled water at gently boiling temperature (about 95°C) for 30 min.

Cycle of Regeneration	Total Amount, mmol		Mole Ratio
	Na^+	Cl^-	
1	1.48	1.39	1.06
2	1.95	1.79	1.09
3	2.00	1.86	1.08
4	1.96	1.79	1.09
5	1.30[a] 0.53[b]	1.19[a] 0.39[b]	1.16[c]
6	1.26[a] 0.64[b]	1.28[a] 0.46[b]	1.09[c]
7	1.64	1.70	0.96
8	1.79	1.93	0.93
9	1.77	1.82	0.94
10	1.84	1.94	0.95
		Avg	1.04

[a]Obtained by washing the sorbent with cold distilled water.

[b]Obtained by leaching the washed sorbent at standard leaching conditions (Fig. 3).

[c]Ratio of the sum of sodium ion to the sum of chloride ion.

To study the effects of pressure and the effects of the moisture content of the flue gas on the sorption performance of both sorbents, a pressurized sorption test unit has been designed. This unit will allow sorption testing of candidate sorbents at up to 10-atm pressure. The engineering drawings of the unit have been completed, and are being reviewed. The items needed for this unit for which delivery times are long have already been ordered. The electrical, water, and ventilation line services needed for the setup of the unit also have been requested.

Table 5. Leachable NaCl in NaCl-Sorbed Activated Bauxite as a Function of Sorption-Regeneration Cycle

Cycle of Sorption and Regeneration	Total Sorbed NaCl,[a] mg	Leachable NaCl,[b] mg	NaCl Leachable, %
1	161	87	54.0
2	147	114	77.6
3	138	117	84.8
4	128	115	89.8
5	123	107	87.0
6	136	111	81.6
7	130	96	73.8
8	132	105	79.5
9	132	103	78.0
10	127	108	85.0
		Cycles 2 to 10, Avg	81.9

[a] From Table 3, row 2.

[b] Calculated from total sodium in leachant (Table 4).

2. Particle Removal from Flue Gas

(W. M. Swift, F. G. Teats, A. R. Pumphrey, S. D. Smith, and J. J. Stockbar)

In PFBC, the hot flue gas from the combustor must be expanded through a gas turbine to recover energy and make the process economic. To prevent erosion of the turbine blades by particles of limestone and fly ash entrained in the flue gas, the particle mass loading must be reduced to acceptably low levels.

Although the air quality requirements for a gas turbine have yet to be experimentally demonstrated, estimates have been made of what constitute "acceptably low levels" of particle mass loading for a gas turbine. Westinghouse, for example, has suggested that loadings in the range of about 0.05 to about 0.005 g/m^3 (depending on the particle size distribution) would be acceptable.[1] Since the particle mass loading in the flue gas leaving the combustor is on the order of about 30 g/m^3, the total particle-removal efficiency required to meet the turbine air-quality requirements would be between 99.8 and 99.98%.

Existing devices readily adaptable to high-temperature, high-pressure particle removal such as conventional cyclones are not very efficient in removing particles with diameters smaller than about 10 μm. Thus, achieving the very low loadings necessary for PFBC requires that highly efficient methods be developed for removing from high-temperature/high-pressure flue gas those particles having diameters between 2 and 10 μm.

Flue gas cleaning methods being tested and evaluated in the off-gas system of the ANL 15.2-cm-dia fluidized-bed combustor include granular-bed filtration and high-efficiency cyclones. Work has been temporarily discontinued on the development of a pulse-jet acoustic dust conditioning system for improved particle removal from a high-temperature/pressure gas stream. Progress in the development of the pulse-jet system was summarized in a previous report (ANL/CEN/FE-79-3). This report presents the results of testing a high-efficiency cyclone.

a. High-Efficiency Cyclone

A Donaldson Co. TAN-JET cyclone, claimed to have better dust-removal efficiency than conventional cyclones, has been installed in the flue gas system of the ANL 15.2-cm-dia pressurized combustor and is undergoing testing and evaluation. The cyclone will also be useful in the testing of the ANL granular-bed filter concept and possibly in the testing of the pulse-jet acoustic dust conditioning concept.

Equipment. Figure 4, which illustrates the present arrangement of the PDU combustion test system, is republished here. Fluidized-bed combustion equipment and instrumentation of the PDU (process development unit) at Argonne includes a 15.2-cm-dia, fluidized-bed combustor that can be operated at pressures up to 1014 kPa, a compressor to provide fluidizing-combustion air, a preheater for the fluidizing-combustion air, peripheral-sealed rotary valve feeders for metering solids into an air stream fed into the combustor, two cyclone separators and a filter (in series) for solids removal from the flue gas, associated heating and cooling arrangements and controls, and temperature- and pressure-sensing and display devices. As is evident in Fig. 4, the TAN-JET cyclone is installed as the secondary cyclone in the PDU flue-gas system.

A schematic of the TAN-JET cyclone is shown in Fig. 5. The TAN-JET employs a secondary flow of clean air to improve gas-solid separation in the primary gas flow. The pressure drop across the secondary air inlet nozzle for the unit being tested is designed to be about 100 kPa. In a commercial application, a TAN-JET would require a booster compressor and air tubes in a PFBC to provide the required flow of clean, high-temperature secondary air.

Experimental Results. The preceding quarterly report presented the results of experiments to measure the TAN-JET cyclone particle-removal efficiency during (1) the fluidization of limestone in the combustor at ambient conditions and (2) the combustion of coal in a fluidized-bed of limestone at 300 kPa and 850°C bed temperature (ANL/CEN/FE-79-3). This report presents (1) an analysis of the previously reported data for the effect on cyclone efficiency of pressure drop across the secondary air inlet nozzle, (2) TAN-JET particle removal efficiency in experiments with coal combusted in a fluidized bed of dolomite at 810 kPa and 870°C bed temperature, and (3) the results of an attempted determination of the TAN-JET size selectivity.

Figures 6, 7, and 8 illustrate, for secondary air nozzle pressure drop values of 70 kPa, 105 kPa, and 140 kPa, respectively, the effect of particle loading in the flue gas entering the TAN-JET cyclone on the penetration and the particle loading of the flue gas leaving the cyclone. The data

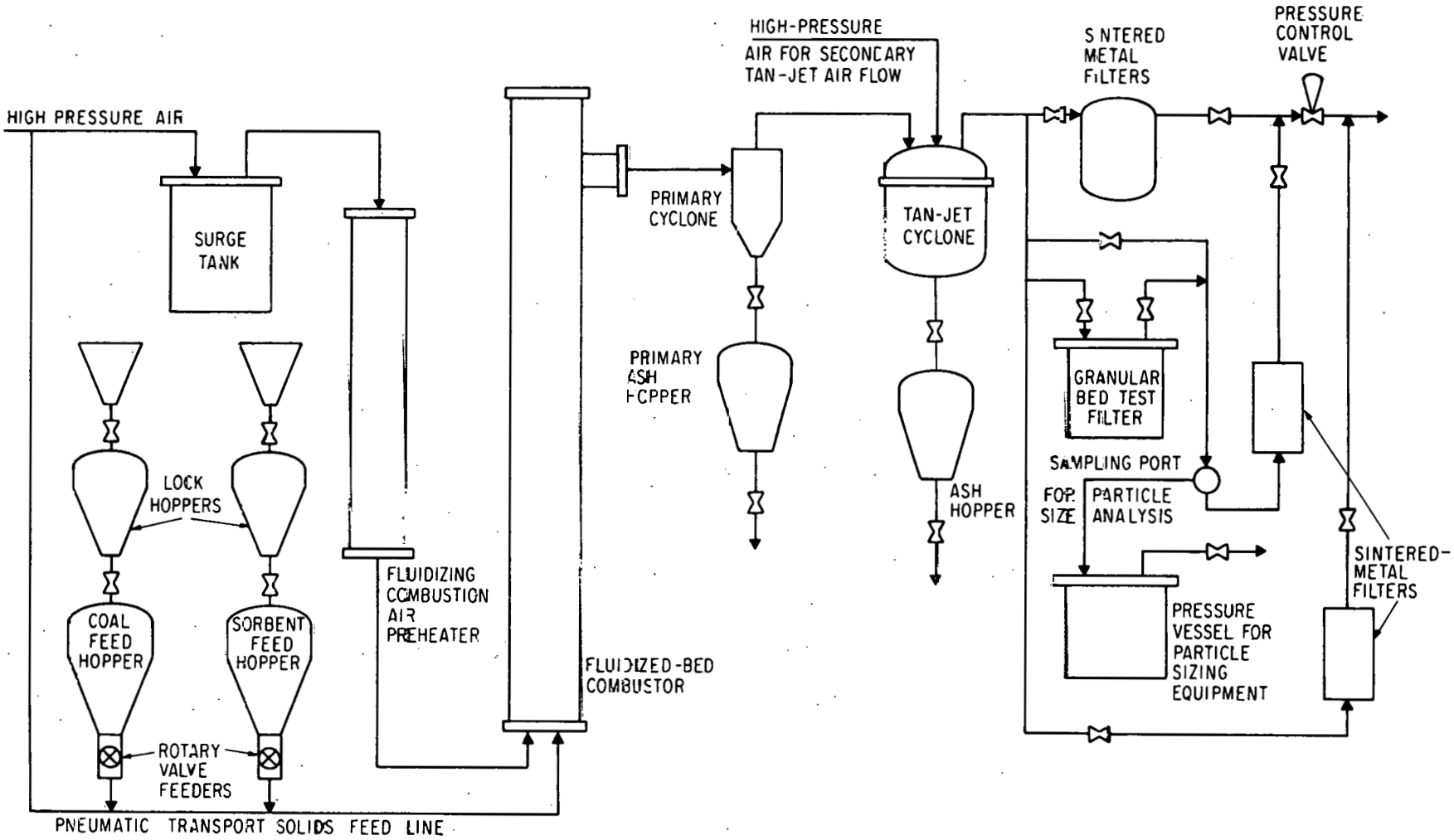

Fig. 4. Schematic Flow Sheet of PFBC System

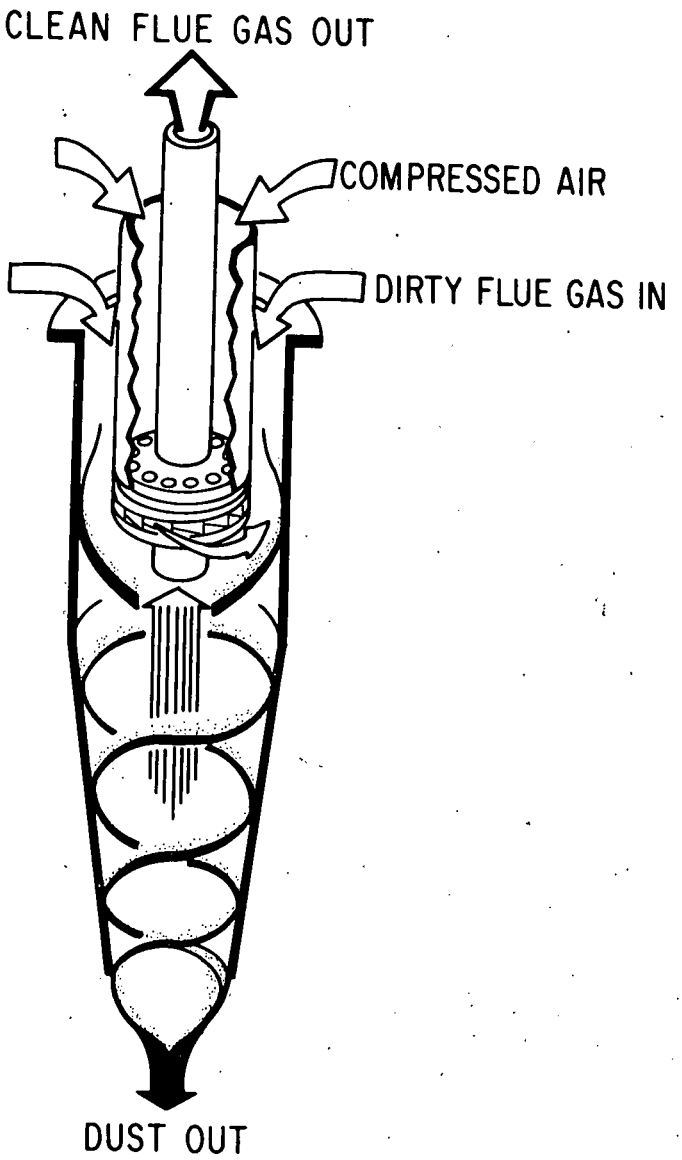

Fig. 5.

TAN-JET Tube Diagram

points are previously reported values obtained during fluidization of limestone in the combustor at ambient conditions and during the combustion of coal in a fluidized bed of limestone at 300 kPa and 850°C bed temperature (ANL/CEN/FE-79-3). Each set of data was correlated using a power curve least squares fit of the form:

$$L_o = aL_i^b$$

where

L_i is the inlet particle loading in g/m^3

L_o is the outlet particle loading in g/m^3

a, b are constants

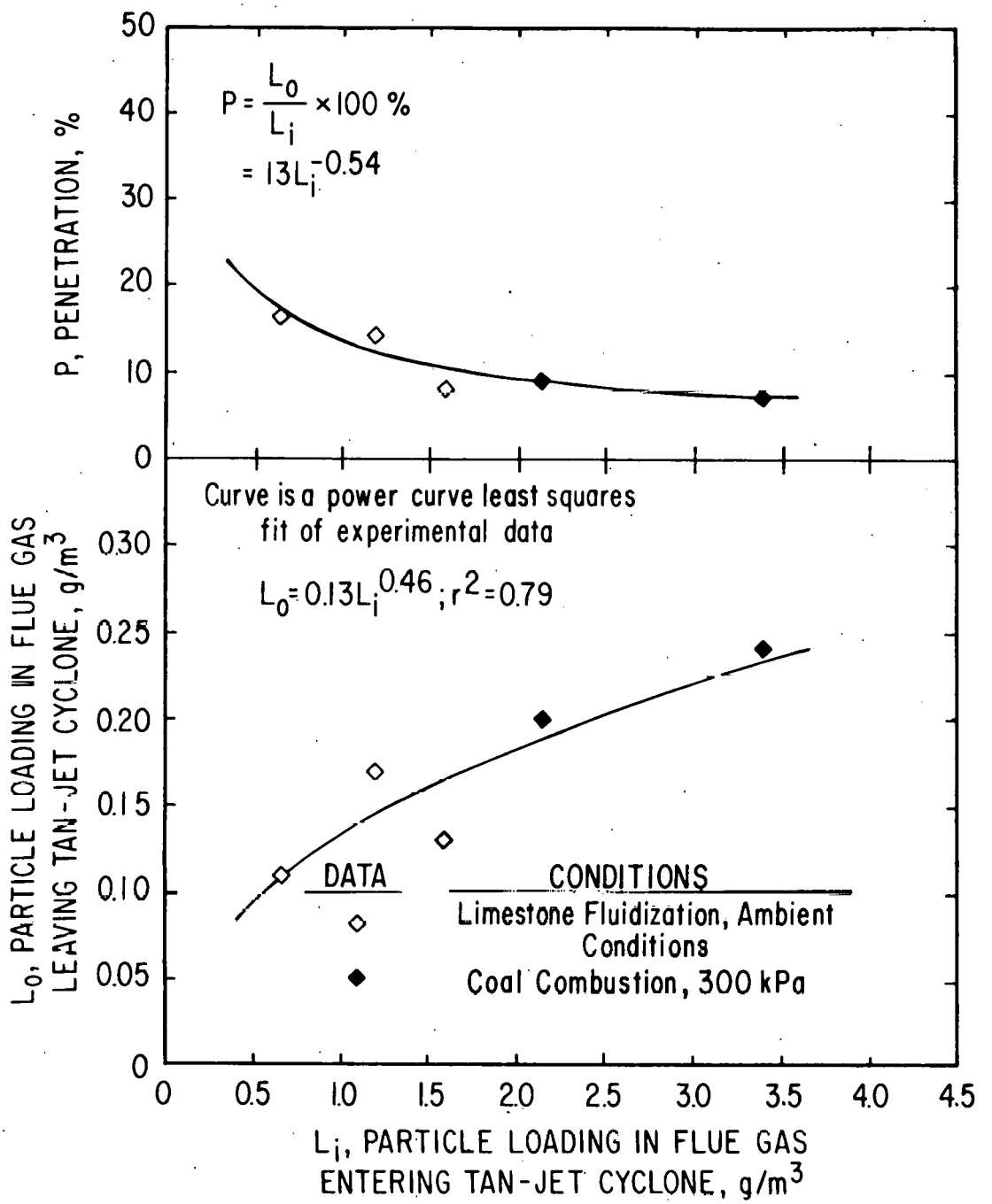

Fig. 6. Penetration and Particle Loading in Flue Gas Leaving TAN-JET Cyclone as a Function of Particle Loading Entering TAN-JET Cyclone for Secondary Air Nozzle. $\Delta P \cong 70$ kPa. See text for definitions of symbols.

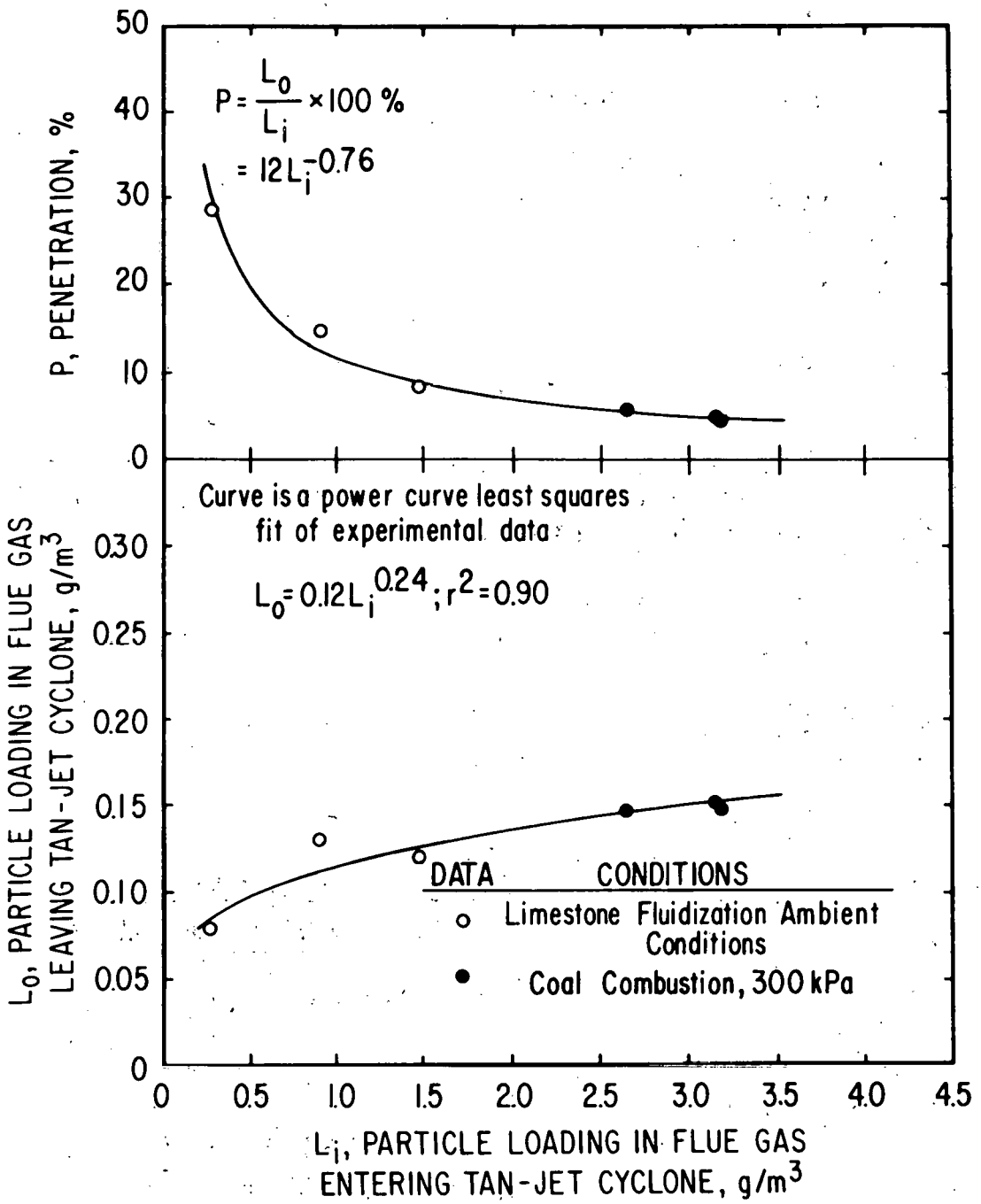

Fig. 7. Penetration and Particle Loading in Flue Gas Leaving TAN-JET Cyclone as a Function of Particle Loading Entering TAN-JET Cyclone for Secondary Air Nozzle. $\Delta P \cong 105$ kPa. See text for definitions of symbols.

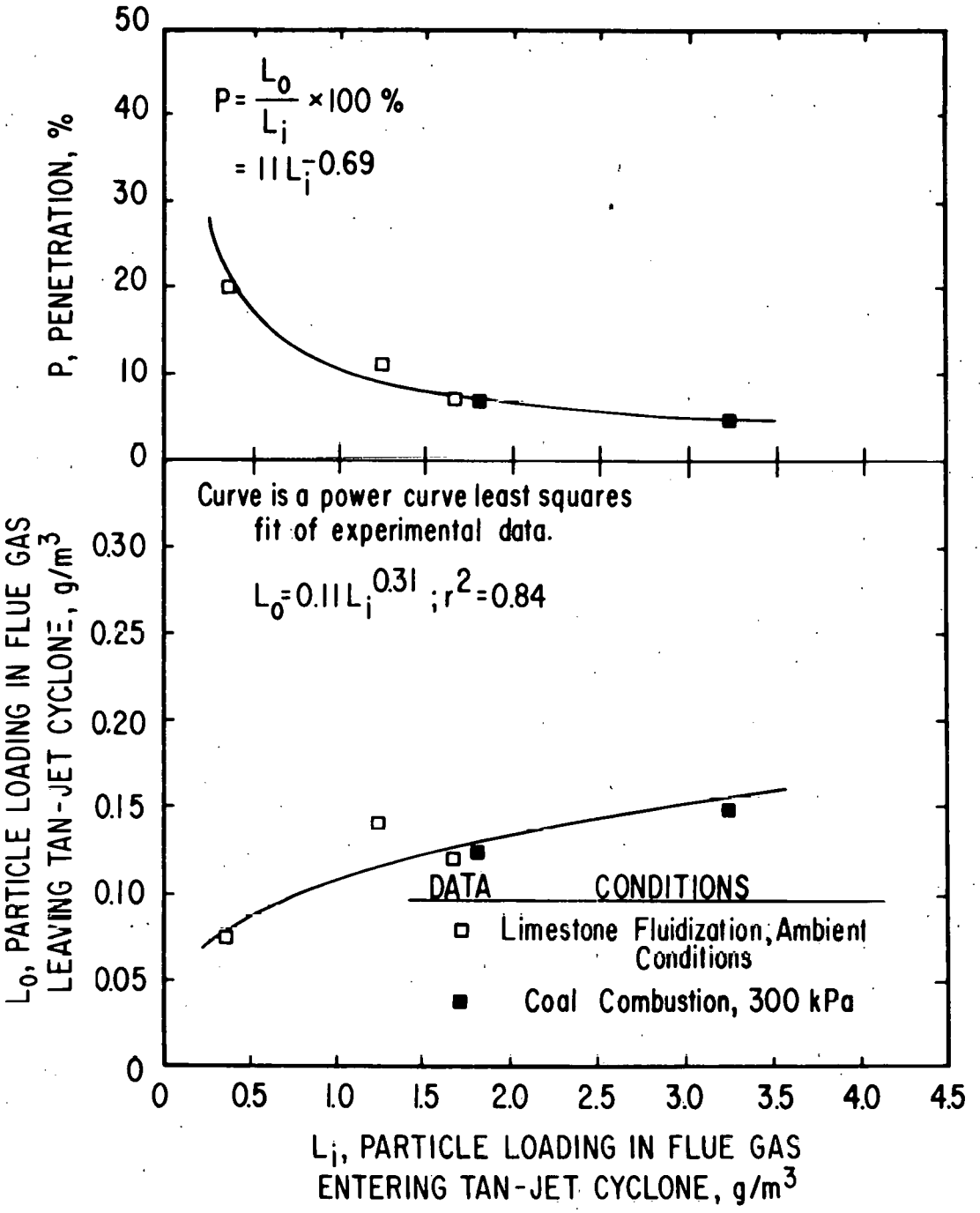

Fig. 8. Penetration and Particle Loading in Flue Gas Leaving TAN-JET Cyclone as a Function of Particle Loading Entering TAN-JET Cyclone for Secondary Air Nozzle. $\Delta P \cong 140$ kPa. See text for definitions of symbols.

Since penetration, P, is simply equal to $(L_o/L_i) \times 100\%$, the equation for the penetration correlation curve is:

$$P = 100\ aL_i^{(b\ -\ 1.0)}$$

The correlation equations and the respective coefficients of determination, r^2, for each correlation are also given in Figs. 6-8.

Figure 9 compares the three independently calculated correlation curves for the three experimental levels of secondary air nozzle pressure drop. The curves for nozzle pressure drops, of 105 and 140 kPa are very similar, indicating that nozzle pressure drop has no effect above the designed operating level of 105 kPa. At the lowest nozzle pressure drop tested (70 kPa), however, the level of particle penetration and the resulting mass loading in the flue gas leaving the TAN-JET were significantly greater than at the higher nozzle pressure drop levels.

Loadings in the flue gas leaving the TAN-JET during operation at a nozzle pressure drop of 105 kPa or 140 kPa and with an inlet loading of 2.5 to 3.5 g/m^3 (typical loadings for experiments with combustion) were on the order of 0.15 g/m^3. Cyclone efficiency (100% minus percent penetration) under these conditions was about 95%. Overall efficiency of the primary and TAN-JET cyclones in series was about 99.5%.

A number of experiments have also been performed to evaluate the performance of the TAN-JET cyclone during the combustion of coal in a fluidized bed of dolomite at 810 kPa and 870°C bed temperature. Following the completion of several experiments at a combustor pressure of 810 kPa and a nozzle pressure drop of 70 kPa in which the solids loadings in the flue gas leaving the TAN-JET cyclone were measured to be unusually high (0.20 to 0.39 g/m^3) for the inlet loading conditions, the cyclone was removed from the pressure vessel and disassembled for examination. At this time, two separate problem areas that potentially affect cyclone performance were discovered.

The first problem concerned plugging of the discharge line between the TAN-JET cyclone and the ash collection hopper. The opening of the discharge line, normally 10 cm in diameter, had been reduced to an about 1.5-cm diameter by accumulation of dust on the wall of the discharge line. Plugging has tentatively been attributed to condensation of moisture during startup, when the metal surface temperatures are below the dew-point temperature of the FBC flue gas. The discharge line of the TAN-JET was wrapped with heating mantles in an attempt to alleviate this problem.

The second area of concern was the discovery of a large quantity of fly ash in the annular space between the TAN-JET cyclone tube and the surrounding pressure shell. The system, designed as a balanced pressure unit, allows the pressure to equilibrate across the cyclone wall as the FBC system pressure is changed. It was evident, however, that dust accumulation in the annular space had resulted from gas leaks in the pressure shell and continuous bleeding of gas from the cyclone into the annular volume. Upon reassembly of the pressure shell, a significant gas leak at the flanged

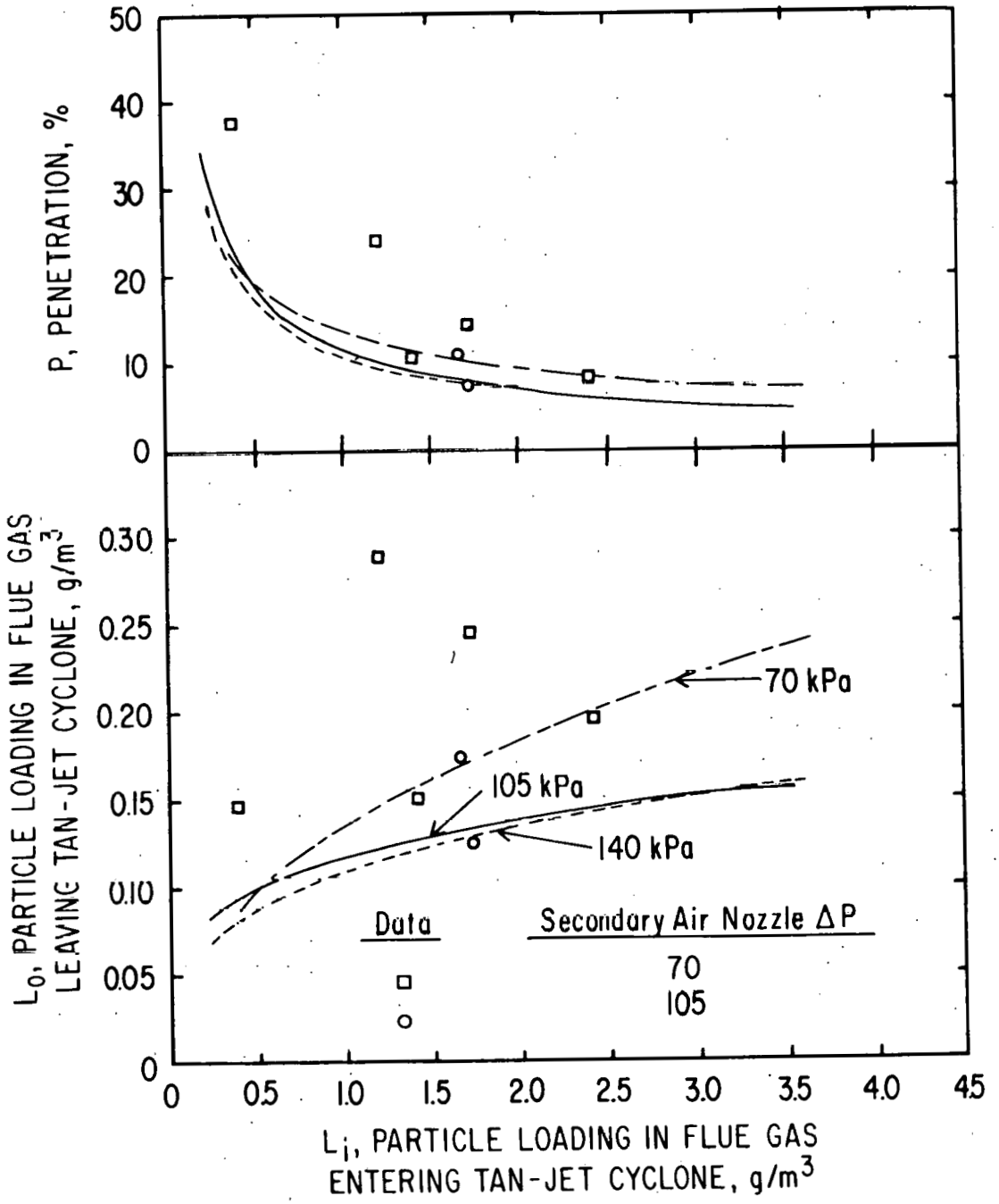

Fig. 9. Penetration and Particle Loading in Flue Gas Leaving TAN-JET Cyclone as a Function of Particle Loading Entering Cyclone. Curves in bottom graph are correlations of data for low-pressure experiments with pressure drops at the secondary air nozzle, ΔP, of 70, 105, and 140 kPa. Data points are for high-pressure (810-kPa) coal combustion experiments.

opening to the unit was confirmed. With the use of new gasketing materials and sealing compounds, the leaks in the pressure shell were reduced considerably.

Following the above modifications, additional experiments were performed to measure TAN-JET particle-removal efficiencies at 810 kPa with coal combustion. The data from these additional tests are given in Fig. 9 where they may be compared with the correlated results of the experiments at ambient and 300-kPa pressure. It is quite evident from the comparison that the performance of the TAN-JET cyclone at high pressure was quite erratic and was inconsistent with the previous results obtained at lower pressure. For example, of the five data points for experiments at 810-kPa system pressure and 70-kPa secondary air nozzle pressure drop, only two are in reasonably good agreement with the correlation for the corresponding low-pressure experiments (broken line in Fig. 9). The other three data points indicate considerably poorer performance (greater penetration and higher loadings leaving the cyclone) than does the correlation curve. Although somewhat poorer performance would be expected from theoretical considerations, both the degree of performance variation and the inconsistency of the results indicate that other factors are responsible. It is suspected that plugging of the ash discharge line between the TAN-JET and the ash receiver hopper continues to be a problem. A new ash receiver is being fabricated to permit the discharge line to be modified in an attempt to improve the consistency of the cyclone performance measurements.

In a first attempt to determine the size selectivity of the TAN-JET (cyclone efficiency as a function of particle size), samples of fly ash recovered from the TAN-JET ash receiver and from a sintered metal filter downstream from the cyclone were analyzed for size distribution by Coulter counter measurement. Representative samples were sent to two independent laboratories ("A" and "B") for comparative analyses. When results were obtained from the laboratories, very large discrepancies were found between the reported distributions for the two samples (about one order of magnitude). This is illustrated in Fig. 10, which compares (1) the Coulter counter analyses from the two laboratories for fly ash recovered from a sintered metal filter downstream from the TAN-JET cyclone with (2) our cascade impactor analysis of flue gas particle size distribution at a point between the TAN-JET cyclone and the filter.

The slope of the Coulter counter distribution from laboratory "B" is similar to that for the flue gas particle size distribution determined by cascade impactor analysis. However, the mass mean particle diameter for the Coulter counter analysis is an order of magnitude greater--about 25 μm as compared with about 3 μm. This could indicate that the fly ash sample was not satisfactorily dispersed in the electrolyte for the Coulter counter analysis.

By comparison, the mass mean diameter (about 1 μm) of the Coulter counter distribution from Laboratory "A" is much closer to that of the impactor distribution. In this comparison, however, the slopes of the distributions are quite dissimilar. It is noted that laboratory "A" reported the distribution to particles as small as about 0.6 μm. Distributions below about 1 μm are difficult to determine with a Coulter counter and are subject to sizable error.

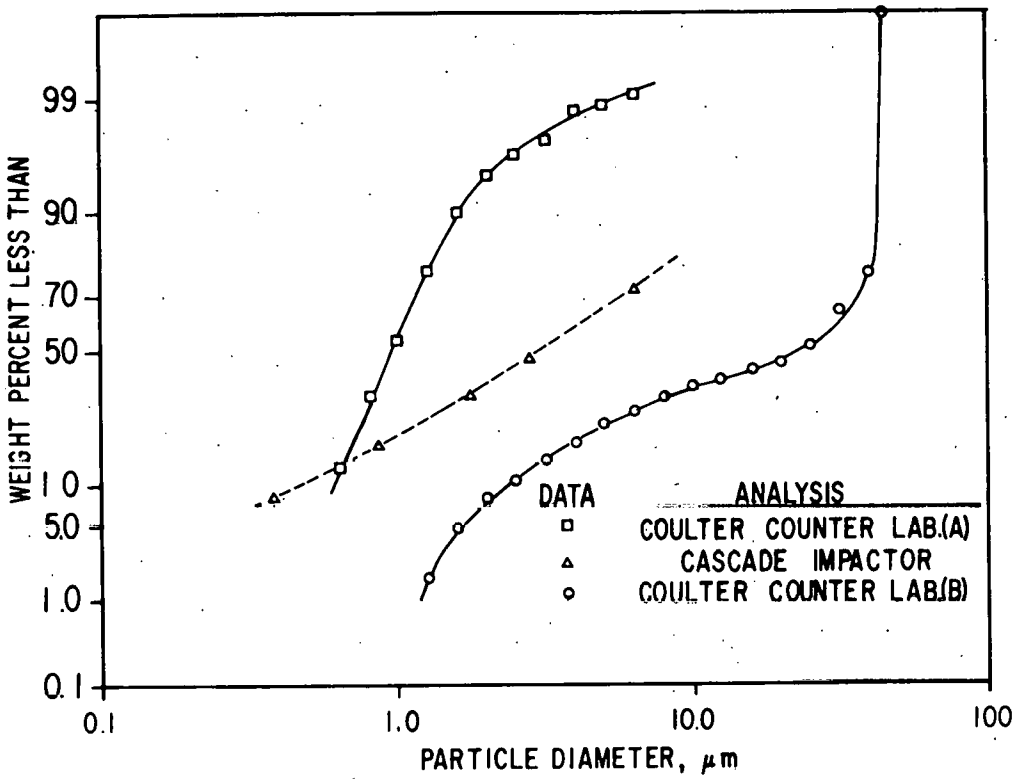

Fig. 10. Cumulative Mass Distributions for Fly Ash Passing Through a TAN-JET Cyclone

As a matter of interest, the two sets of Coulter counter data were used to generate size selectivity curves for the TAN-JET cyclone. To develop composite distributions (not shown) for the fly ash entering the cyclone, the size distributions of material from the sintered filter (Fig. 10) were combined with their respective distributions (not shown) for fly ash recovered from the TAN-JET ash receiver. The two independent sets of data were then used to develop size selectivity curves for the TAN-JET cyclone which illustrate the cyclone particle-removal efficiency of the cyclone as a function of particle diameter. The results are given in Fig. 11 along with the theoretical cyclone efficiency curve supplied by Donaldson Co., developer of the TAN-JET.

Two important parameters which help to characterize cyclone performance and which can be obtained from the curves in Fig. 11, are cut size, $(dp)_{50}$, and the sharpness index, $(dp)_{25}/(dp)_{75}$, where $(dp)_n$ corresponds to the particle size having a size selectivity of n percent.

Table 6 lists the values for cut size and sharpness index from the three curves in Fig. 11. For high-efficiency cyclones, a low cut size and a high sharpness index are desirable characteristics.

It is impossible, of course, to make any conclusions regarding the performance of the cyclone based on the numbers in Table 6 because of the vast descrepancy in the measured parameters. Efforts are continuing, however, to obtain more reliable estimates of cyclone performance.

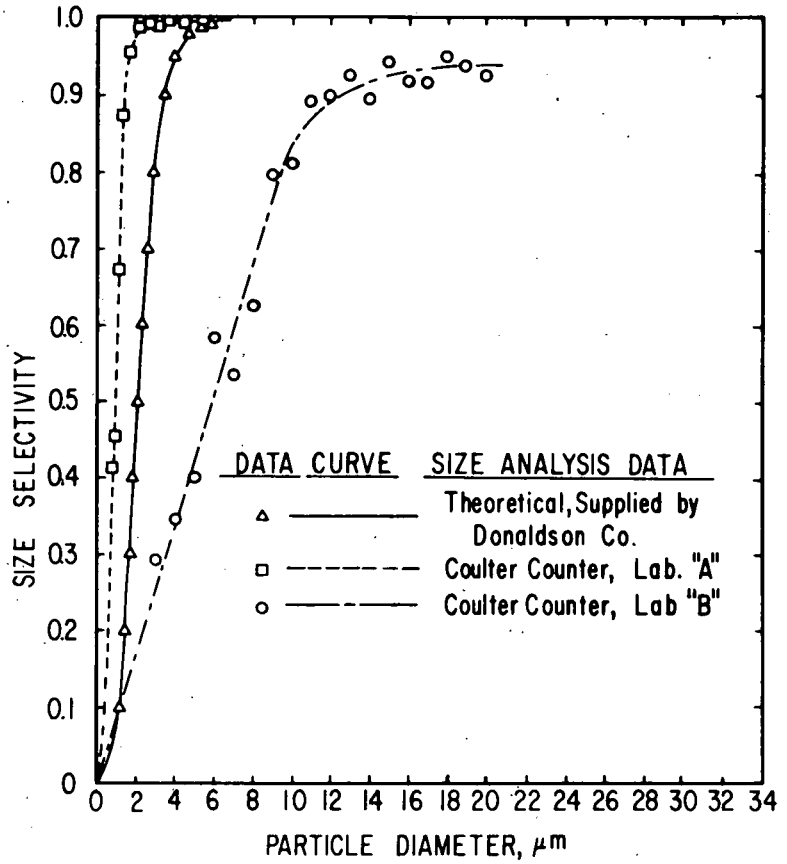

Fig. 11. Size Selectivity Curve for TAN-JET Cyclone

Table 6. TAN-JET Performance Parameters

Size Selectivity Data Basis	Cut Size, μm	Sharpness Index
Coulter Counter, Lab "A"	0.9	0.53
Theoretical	2.1	0.56
Coulter Counter, Lab "B"	5.9	0.33

TASK B. TRACE POLLUTANTS

1. Assessment of Particulate Emissions from Atmospheric Fluidized-Bed Combustors

(E. B. Smyk)

Atmospheric fluidized-bed combustion (AFBC) is a technology by which coal can be burned to generate electric power and/or steam while meeting EPA SO_2 and NO_x emission regulations with no add-on equipment. However, AFBC must also meet particulate emission regulations. In order to design adequate control devices, these emissions must be analyzed and characterized.

a. Dust Loading

In general, the dust loading from AFBC has been found to be higher than that from conventional pulverized-coal (PC) firing. However, the dust loading from an AFBC is quite variable and can vary over a much greater range than PC emissions. The following operating parameters have been found to affect the dust loading from an AFBC: temperature, superficial gas velocity, presence and arrangement of cooling tubes in the bed, calcium to sulfur (Ca/S) mole ratio between the sorbent and the coal, coal size, sulfur content and ash content, sorbent type and particle size, and combustion efficiency. Most of these variables are interrelated and each is discussed below.

Temperature. Although temperature has little direct effect on dust loading, it may affect both the Ca/S ratio selected and the combustion efficiency. Optimum SO_2 retention occurs approximately midway in the possible operating temperature range of AFBC (1000-1250 K). Therefore, employing high or low temperatures would necessitate higher Ca/S ratios to meet SO_2 emission regulations. As is discussed below, Ca/S ratio may have an effect on dust loading.

Higher temperatures generally lead to more efficient combustion. Since a large portion of the unburned carbon elutriates from the bed, temperature has an indirect effect on dust loading.

Superficial Gas Velocity. Superficial gas velocity is probably the single most important parameter in determining dust loading. High velocities tend to increase dust loading for three reasons: (1) small particles are elutriated when gas velocity rises above the terminal velocity of these particles, (2) increased gas velocity results in more agitated conditions in the bed, with attrition increasing as a result of more violent contact between particles, and (3) increased gas velocity usually results in decreased combustion efficiency. The unburned carbon particles, usually quite small, tend to elutriate and to show up as particulate emissions.

Presence of Cooling Tubes. The presence of cooling tubes in a bed tends to decrease bed turbulence, to postpone the onset of "slugging," and generally to decrease particulate emissions.

Ca/S Ratio. Ca/S ratio has two effects on particulate emissions. First, at a higher Ca/S ratio, more sorbent is cycled through the bed. At a lower Ca/S ratio, although the amount of sorbent present at any one time does not change, there is less attrition since the attrition rate of sorbent decreases with time. Therefore, at a higher Ca/S ratio, the rate of attrition (and thus particulate emissions) is higher. Second, at a higher Ca/S ratio, there is more unreacted stone in the system. Since sulfation tends to harden the stone and make it less prone to attrition, there is greater particulate emission at a higher Ca/S ratio.

Coal Properties. The coal properties relevant to assessing particulate emissions are particle size, ash content, and sulfur content. The smaller the original coal particles, the smaller the resulting unburned carbon and ash particles and the more likely they are to elutriate. Also, when coals with higher sulfur contents are burned, more sorbent must be fed and this tends to increase partculate emissions.

Sorbent Properties. Sorbent reactivity, hardness, and size are important to assessing potential particulate emissions. The more reactive a sorbent, the less needs to be fed to meet SO_2 emission regulations. A more reactive stone also is sulfated to a greater degree, which hardens the stone and makes it more attrition-resistant. Both of these factors decrease particulate emissions. The use of a stone which is fundamentally harder and thus more attrition-resistant should also result in lower particulate emissions. However, the attrition resistance of a stone is not only a function of its hardness. Some otherwise hard stones decrepitate rather severely when fed to an AFBC; the reasons for this are not fully known. If a sorbent with a high fines contact is fed to a combustor, much of the material will elutriate, increasing the particulate emissions.

Combustion Efficiency. Combustion efficiency affects particulate emissions in two ways. First, most of the unburned coal consists of small carbon particles which are elutriated. Second, since the sulfur contained in the coal burns preferentially, most of the sulfur in the coal is released as SO_2, even if some of the carbon remains unburned. Thus, for a given heat output, sulfur emissions are increased at lower combustion efficiencies and more sorbent must be fed to the combustor to limit these. Low combustion efficiency may also increase particulate emissions for reasons related to coal sulfur content and Ca/S ratio.

b. Particle Size Distribution

The particle size distribution of particulate emission from an AFBC has not been extensively measured, but the general feeling is that the particles from AFBC are somewhat coarser than those from PC firing. That is, the effluent from AFBC has greater amounts of coarse particles and fewer fine particles than the PC effluent. Methods of predicting particle size distributions from operating parameters are presently unavailable, and work needs to be done in this area.

c. Composition of Particulate Emissions

The particulates emitted from AFBC comprise three categories: unburned carbon, coal ash, and partially sulfated sorbent. In general, most of the unburned carbon and ash are elutriated from a bed. The quantity of partially sulfated sorbent elutriated from a bed depends on all of the parameters discussed in the previous section.

Because of the low combustion temperature used in AFBC, the unburned carbon fraction may also contain condensed polycyclic aromatic hydrocarbons (PAH), as well as other hydrocarbon derivatives, although the hydrocarbon derivatives are more likely to be present in the vapor fraction. These compounds are of interest because some of them are carcinogenic and may be present in AFBC effluent in greater concentrations than in PC effluent.

The coal ash portion of AFBC effluent is chemically similar to that of PC effluent, i.e., it is a mixture of metal oxides, most notably those of calcium, magnesium, sodium, potassium, aluminum, silicon, and iron. However, PC ash but not AFBC ash has generally been sintered (melted and recondensed). The AFBC ash thus tends to be softer, more porous, and less "glassy." Different ashes contain differing amounts of "trace" elements such as mercury, arsenic, lead, cadmium, boron, bismuth, fluorine, selenium, vanadium, antimony, etc. These elements have toxic properties, and care should be taken to minimize their contamination of the environment. Work to date seems to indicate that the emission of trace elements is lower in AFBC than in PC. In addition, the tendency of trace elements to preferentially deposit on the finer particles seems to be more prevalent in PC than in AFBC.

Elutriated partially sulfated sorbent contains magnesium and calcium oxides and carbonates and calcium sulfate, as well as the impurities contained in the original sorbent. The compositions of these impurities and of coal ash are in general similar. Elutriated sorbent is generally sulfated to a greater extent than is the sorbent that remains in the bed.

d. Methods of Meeting Particulate Emission Regulations in AFBC

Before a system can be designed to control particulate emissions from AFBC, the resistivity of particles in the stream must be known. Also dust loading and particle size distribution have already been discussed and are very important.

If an electrostatic precipitator (ESP) installation is being considered, the resistivity of the particles must be considered. ESPs function optimally if particle resistivity is in a range between 10^7 and 10^{10} Ω-cm. The resistivity of the partially sulfated sorbent is on the order of 10^{12} Ω-cm. The resistivity of coal ash is also too high for proper collection since very little if any SO_2 is present in AFBC flue gas. There is disagreement as to how unburned carbon particles would affect the collection efficiency of an ESP. Carbon is a good conductor; however, the reported measurement (resistivity of 3.5×10^{-3} Ω-cm) was probably made with a crystalline graphite block rather than the small amorphous carbon particles present in flue gas. Therefore, how unburned carbon particles are really collected in an ESP is open to question.

It has also been proposed that materials with low and high resistivities be mixed to produce a material which can be collected in an ESP. This seems doubtful since precipitation is essentially a single-particle phenomena and the resistivities of separate particles cannot be averaged to obtain a "characterization resistivity" of the entire system.

It has usually been agreed that one or preferably two stages of conventional cyclones should precede the final particulate-control device. A cold (425 K) ESP would almost certainly be ineffective and even a hot (600 to 700 K) ESP might not work because of the high particle resistivities. Flue gas conditioning (adding trace amounts of SO_3 to the flue gas) to decrease the resistivity of the particles has not been studied in relation to AFBC. This technique might make use of ESPs possible.

As an alternative, bag houses may be used as particulate control devices. This is a promising new technique and has only recently been applied to utility-scale applications. However, no AFBC unit with a bag house has been tested.

e. Conclusions

In general (in comparison with PC firing), AFBC produces a considerably greater dust loading of coarser particles having higher resistivity. These characteristics can very widely with the specific operating parameters of the AFBC unit. AFBC particulate emissions have been analyzed and characterized to some degree, mostly on small units, but much work must be done on large (at least pilot-scale) units before a particulate control system can be designed with confidence.

TACK C. LIMESTONE UTILIZATION

1. Enhancement of Limestone Sulfation

(J. A. Shearer, C. B. Turner, and W. I. Wilson)

The addition of inorganic additives to limestones in fluidized-bed coal combustion to enhance SO_2 removal from the off-gases is being evaluated. Most of the work has dealt with the effects of sodium chloride addition on enhancement of the sulfation of limestones and dolomites. Calcium chloride has also been investigated with promising results, as have other inorganic salts.

a. Effect of $CaCl_2$ on Particle Structure of Limestone

As part of this study, scanning electron microphotographs were taken for visual confirmation of structural changes indicated by previous porosimetry measurements. Figure 12 shows calcite spar which has been calcined after a very small addition of $CaCl_2$. The intent here was to isolate individual particles of the salt and to note the effects on the limestone at the site of salt deposition. This figure shows one such site that illustrates the intense recrystallization occurring during calcination when $CaCl_2$ is present. The salt's effectiveness decreases from the point of contact and appears to follow structural lines of the original rhombic calcite particle. The effect on pore structure is evident--even at a distance from the point of immediate contact. Initial melting of the $CaCl_2$ strongly affected the stone at the point of contact. As a result, a single large crystal of CaO formed having visible growth rings as in Fig. 12(b).

Figure 13 is a series of photographs of ANL-9701 stone calcined with various amounts of $CaCl_2$ and illustrating the same structural changes as in calcite, but modified by the impurities and the less crystalline nature of this limestone. At the highest concentrations of salt (1.0 mol % $CaCl_2$), crystal growth begins to be evident, as well as initial fusion of particles. This fusion is a result of there being sufficient $CaCl_2$ liquid to dissolve substantial amounts of CaO, with subsequent loss of structural integrity. At this level of salt addition, conversion to $CaSO_4$ does not depend on the space created by initial decarbonation but can extend indefinitely since dissolution of CaO and loss of structural integrity make the CaO readily available for sulfation.

b. Effect of NaCl on Particle Structure of Limestone

In the case of NaCl, substantial solution of CaO does not occur upon the addition of large amounts of salt to a structure that is still space restrictive to $CaSO_4$ formation beyond about 50% conversion.

Figure 14 is a series of photographs showing the effect of sodium chloride on a previously sulfated sample of ANL-9501 stone (Grove limestone). Figures 14-I and 14-Ia show a sample of untreated ANL-9501 stone completely sulfated at 850°C with 0.3% SO_2; a dense layer of $CaSO_4$ formed at the particle surface, as indicated by the sulfur scan in Fig. 14-Ia. Figure 14-II shows this same sample after treatment with a small amount of powdered NaCl

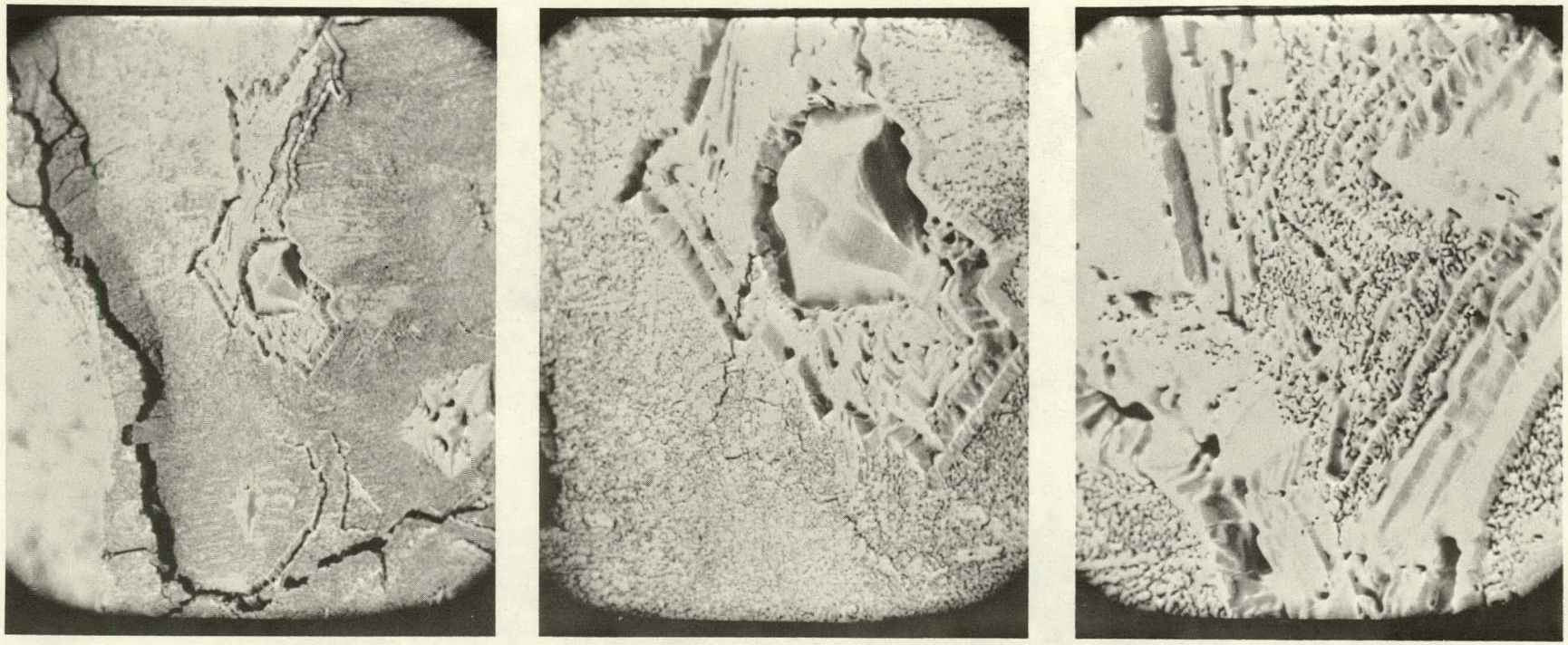

a
181X

b
451X

c
902X

Fig. 12. Cross Sections of Calcite Spar Calcined with 0.05 mol % $CaCl_2$ at 850°C in 5% O_2, CO_2, and the Balance N_2. ANL Neg. No. 308-78-639

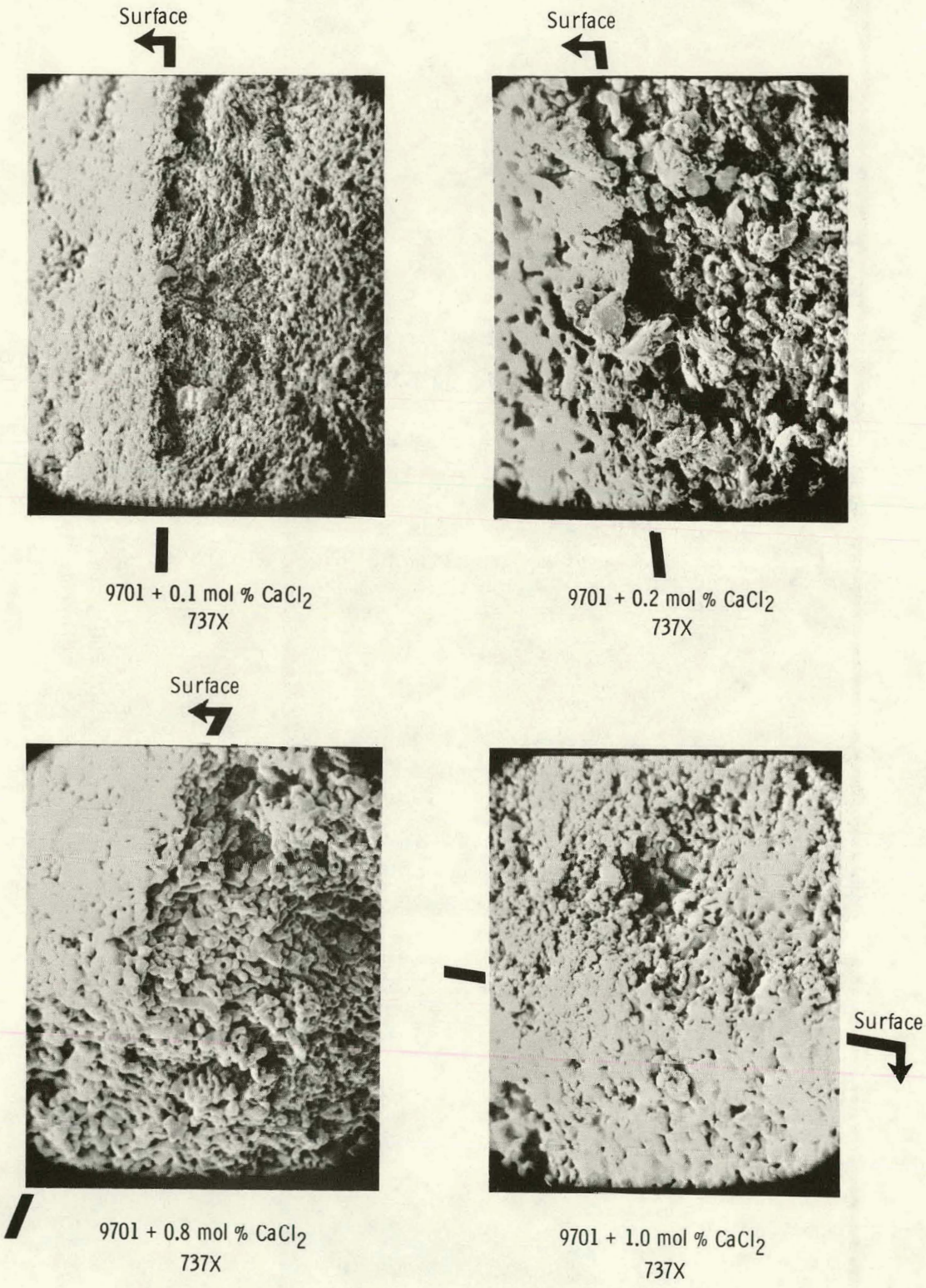

Fig. 13. Effect of $CaCl_2$ on ANL-9701 Stone (Cross Sections) Calcined at 850°C for 1 h in 5% O_2, 20% CO_2, and the Balance N_2. ANL Neg. No. 308-78-640

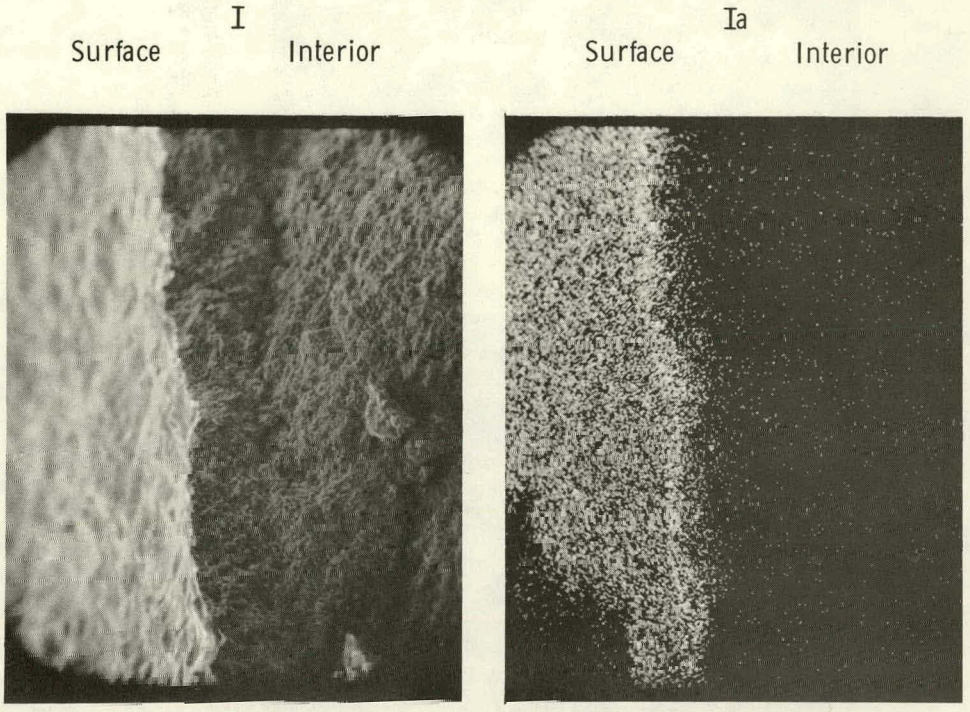

9501 Calcined 1 h
Sulfated 2 h
Reheated 2 h
385X

Sulfur Scan
of I
385X

Fig. 14. The Effects of Heating with NaCl on ANL-9501 Stone (Cross Sections) Previously Sulfated at 850°C for 6 h in 0.3% SO_2, 5% O_2, 20% CO_2, and the Balance N_2. ANL Neg. No. 308-78-758

II

Surface Interior

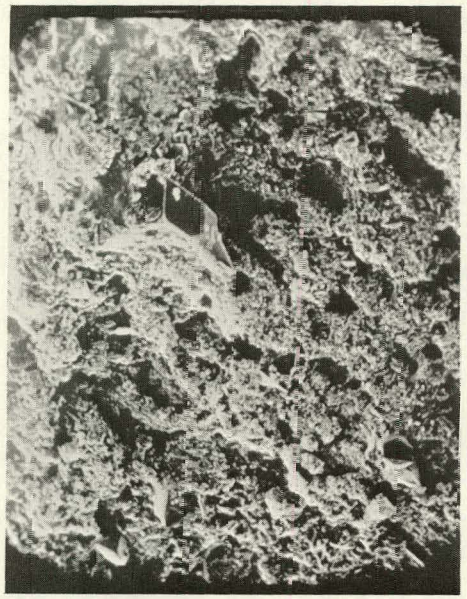

9501 Calcined 1 h
Sulfated 2 h
Reheated with NaCl 2 h
385X

IIa

Surface Interior

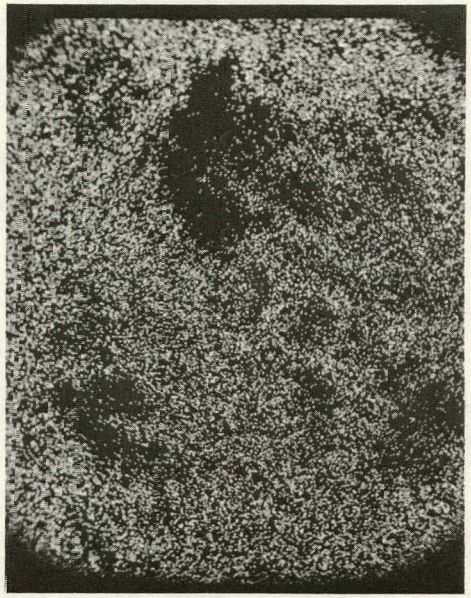

Sulfur Scan
of II
385X

III

Surface Interior

9501 Calcined 1 h
Sulfated 2 h
Reheated with NaCl 2 h
770X

Fig. 14. (Contd)

and reheating. The structure definitely altered and pores are much larger. Figure 14-IIa shows the deep penetration of sulfur into the stone. The enhanced mobility of the system contributed by the low-melting salt caused the $CaSO_4$ to migrate to the particle interior and to undergo massive recrystallization as shown in the closeup (Fig. 14-III). This phenomenon explains the effects of NaCl in renewing the sulfur-removing capabilities of spent bed material as reported by Pope, Evans, and Robbins.[2] The dense diffusion-limiting layer of $CaSO_4$ is no longer intact in the treated material and, with major growth in pore size, there is a more favorable pore distribution for further sulfur capture.

c. Effect of Calcium Chloride on Sulfation of and Particle Structure of Dolomites

The experimental work with enhancement agents has been primarily concerned with limestones, but dolomites also are under consideration as sulfur-capturing species. Since some dolomites are very unreactive, addition of inorganic salts to these systems to increase their reactivity may be of interest. Most dolomites react readily with SO_2--apparently because at the conditions existing in a fluidized-bed coal combustor, the porosity of the stones is enhanced by decomposition of $MgCO_3$ to form MgO, which is unreactive with SO_2.

Horizontal tube furnaces supplied with a simulated flue gas are being used to establish sulfation capacities for a series of precalcined dolomites treated with $CaCl_2$. Porosimetry measurements on similarly prepared calcines are also currently under way. Table 7 lists percent conversions for several stones treated with 0, 0.1, 0.5, 1.0, 3.0, and 5.0 mol % $CaCl_2$ (treated by adding and evaporating an aqueous slurry). The percent conversions were arrived at from final weight-change measurements and are subject to correction when analyses for sulfate are complete. The data show that salt addition tends to enhance sulfation--both at low concentrations (0.1 to 0.5 mol %) and at higher concentrations ($\geq$3.0 mol %). Conversions are lower at the intermediate salt addition. The lowering of conversion at an intermediate salt addition has been ascribed to the initial increase in porosity (by increased ionic mobility) becoming offset by a concomitant decrease in surface area. The second gradual increase in conversion is due to dissolution of CaO in the large amount of liquid salt present, creating an especially reactive situation for sulfation which is not suppressed by structural restrictions.

Figures 15-17 show scanning electron microphotographs of dolomites treated with several concentrations of $CaCl_2$. They illustrate that with very high concentrations of salt (as in Fig. 17 with 5 mol % $CaCl_2$) there is a dramatic increase in average pore size and fused structures develop. Even a trace of $CaCl_2$ (0.1 mol %) causes noticeable pore enlargement, increasing the sulfation capacity of the stones. Dolomite ANL-5601 is an especially unreactive stone of microporous original state which responds to salt treatment with dramatic pore enlargement and consequent enhanced sulfation. This type of highly crystalline stone, which produces a calcine having very small pores, is the sort of dolomite that is benefitted most by salt addition, which affects the pore size of the calcined stone. Very reactive stones do not show as great a percent increase in reactivity although the enhancement of rate

Table 7. Conversion of CaO to $CaSO_4$ for Dolomites Treated with Calcium Chloride

Stone Designation	Percent Conversion, CaO to $CaSO_4$[a]					
	Untreated Stone	0.1 mol % $CaCl_2$ Added	0.5 mol % $CaCl_2$ Added	1.0 mol % $CaCl_2$ Added	3.0 mol % $CaCl_2$ Added	5.0 mol % $CaCl_2$ Added
ANL-4801	79.7	>100.00	99.4	80.8	72.3	89.7
ANL-4902	92.0	>100.00	94.0	70.9	69.7	77.1
ANL-4903	77.9	83.9	82.2	76.9	77.8	97.8
ANL-5101[b]	88.6	99.3	96.8	88.6	85.8	90.7
ANL-5102	76.7	79.8	71.7	67.3	81.7	93.6
ANL-5201	76.0	80.7	76.6	58.7	55.1	88.7
ANL-5207	46.3	48.8	35.7	49.6	55.9	64.5
ANL-5501	31.0	33.9	38.7	37.1	43.9	54.5
ANL-5601	18.1	23.8	54.6	46.8	56.1	57.0

[a]All stones calcined for 1 h at 850°C in 5% O_2, 20% CO_2, and the balance N_2, and sulfated in 0.3% SO_2, 5% O_2, 20% CO_2, and the balance N_2 for 6 h at 850°C.

[b]Tymochtee dolomite.

of reaction achievable by salt addition may be important in a commercial-scale combustor system. For dolomites, enhancement by $CaCl_2$ with very high salt additions can lead to almost complete sulfation of the CaO component.

A plot of conversion versus average pore diameter is being prepared for dolomites (both $CaCl_2$-treated stones and NaCl-treated stones). Also, SEMs being taken of all dolomite calcines studied will be added to a file on limestone and dolomite characterization.

5101 Calcined 1h 850°C
638X

5101 + 0.1 mol % $CaCl_2$
Calcined 1h 850°C
638X

5101 + 2.0 mol % $CaCl_2$
Calcined 1h 850°C
638X

5101 + 5.0 mol % $CaCl_2$
Calcined 1h 850°C
638X

Fig. 15. Cross Sections of Untreated ANL-5101 Dolomite Particles and Particles Treated with $CaCl_2$ at 850°C. ANL Neg. No. 308-78-684

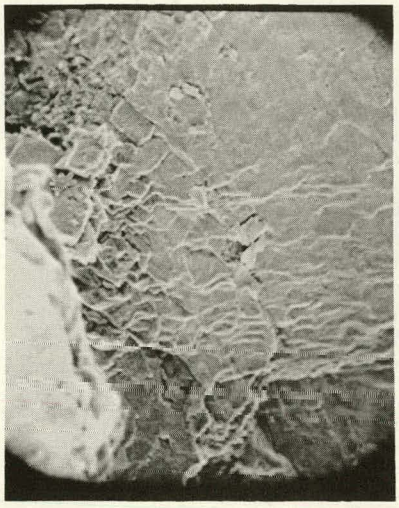

5401 Calcined
1h 850°C
1276X

5401 + 0.1 mol % $CaCl_2$
Calcined 1h 850°C
1276X

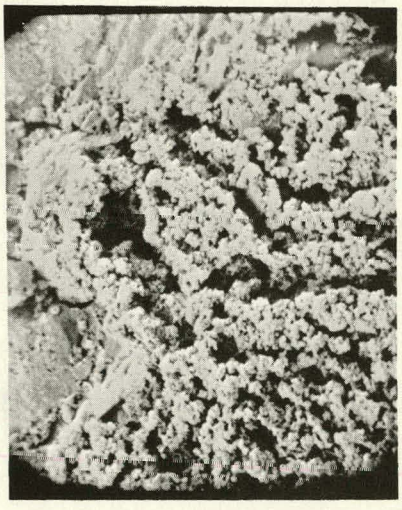

5401 + 0.5 mol % $CaCl_2$
Calcined 1h 850°C
1276X

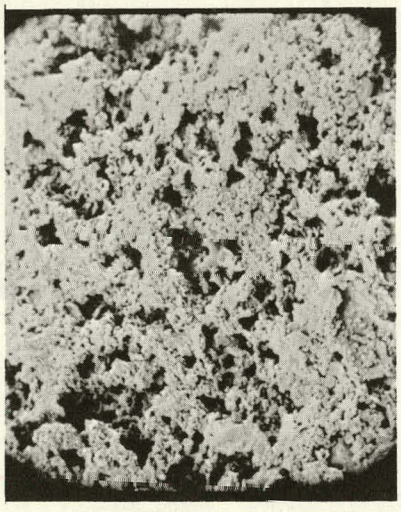

5401 + 3 mol % $CaCl_2$
Calcined 1h 850°C
1276X

5401 + 5 mol % $CaCl_2$
Calcined 1h 850°C
1276X

Fig. 16. Cross Sections of Untreated ANL-5401 Dolomite Particles and Particles Treated with $CaCl_2$ at 850°C. ANL Neg. No. 308-78-685

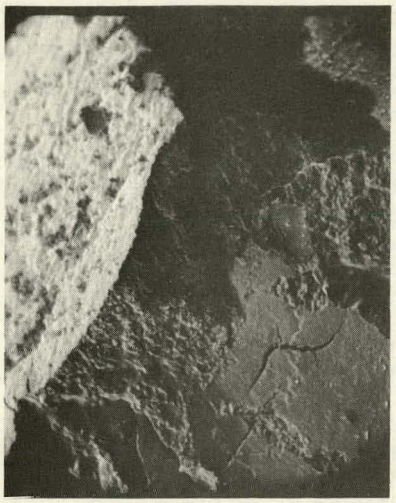

5601 Calcined
1h 850°C
638X

5601 + 0.1 mol % $CaCl_2$
Calcined 1h 850°C
638X

5601 + 0.5 mol % $CaCl_2$
Calcined 1h 850°C
638X

5601 + 1.0 mol % $CaCl_2$
Calcined 1h 850°C
638X

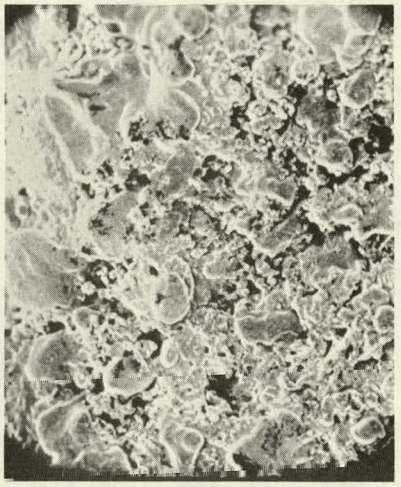

5601 + 5.0 mol % $CaCl_2$
Calcined 1h 850°C
638X

Fig. 17. Cross Sections of Untreated ANL-5601 Dolomite Particles and Particles Treated with $CaCl_2$ at 850°C. ANL Neg. No. 308-78-683

d. Effect of Na_2CO_3 on Sulfation of Limestones

In addition to sodium chloride and calcium chloride, other salts were investigated for possible positive effects on sulfation of limestone. It had been found in materials corrosion studies that the major attack by NaCl and $CaCl_2$ was through the chloride ion (ANL/CEN/FE-78-10). Sodium carbonate had shown promising effects in some early screening experiments. Since Na_2CO_3 contains no chloride, it is hoped that this salt would cause considerably less corrosion of materials in a fluidized-bed coal combustor.

Figure 18 presents a bar graph summarizing the data for three limestones treated with various amounts of Na_2CO_3. Also included are data for ANL-8001 stone treated with Na_2CO_3 and then simultaneously calcined and sulfated; in contrast, the rest of the sulfation is for precalcined material, as is most of the data presented for other salts. The data show marked positive effects due to small additions of Na_2CO_3 on all three stones. The effects occurred most readily in ANL-8001 stone, which has the highest impurity content and the smallest initial grain size. However, under simultaneous calcination/sulfation conditions, the same stone requires a much larger amount of salt to obtain the same conversion.

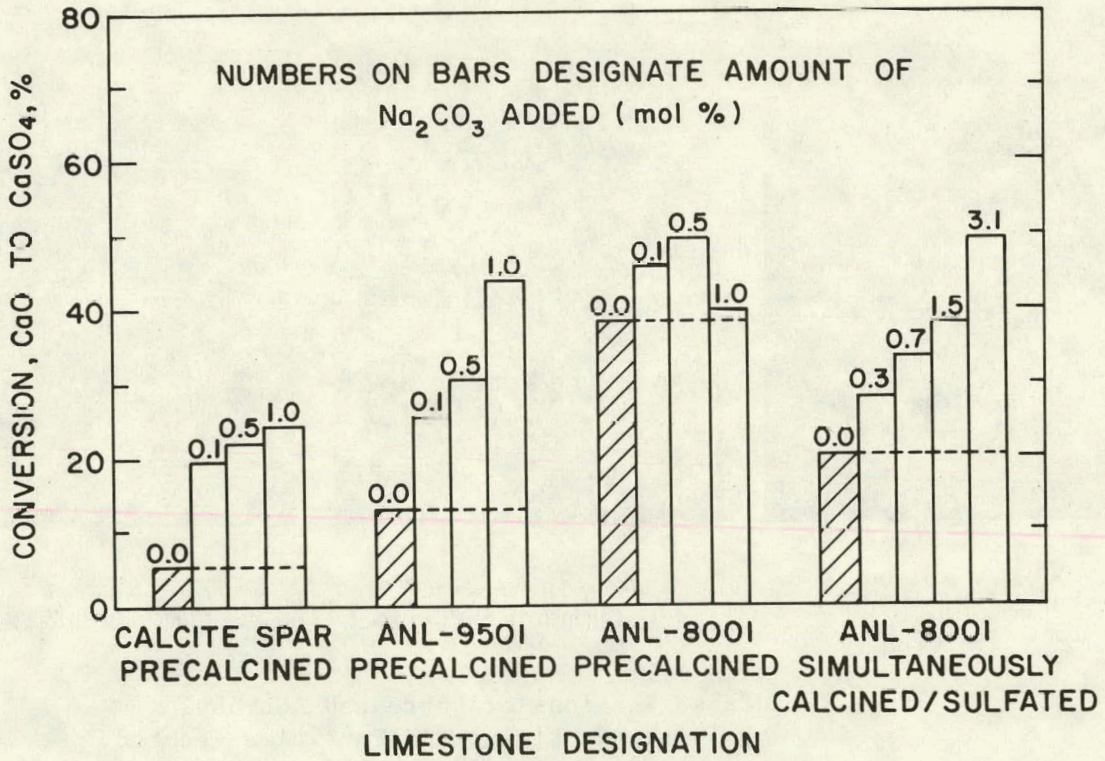

Fig. 18. Effect of Na_2CO_3 on Sulfation of Limestone at 850°C in 0.3% SO_2, 5% O_2, 20% CO_2, and the Balance N_2

Large-scale use of NaCl, $CaCl_2$, and Na_2CO_3 in a fluidized-bed coal combustor are presently under way in conjunction with corrosion testing of materials. The effects of large amounts of coal ash are unknown since in the laboratory-scale experiments, simulated flue gas, not flue gas from coal combustion, has been used.

e. Effect of Temperature on Simulation Enhancement and Sulfation Rate

In conjunction with the salt additive work in horizontal tube furnaces, a series of TGA runs were made to investigate the effects of temperature on sulfation enhancement and rate of sulfation of limestone ANL-9501 (Grove). Figures 19 and 20 are bar graph plots of the sulfation data for NaCl-treated ANL-9501 and $CaCl_2$-treated ANL-9501 stones, respectively. Also shown in each case are conversions for untreated limestone at each temperature. These were all precalcined at the temperature of sulfation. For both salts, there is a pronounced decrease in sulfation in the 850-900°C range and very high sulfations at lower temperatures. At high temperatures (>900°C), the salt-treated samples show much greater sulfation compared to the untreated stones due to the increased dissolution of CaO.

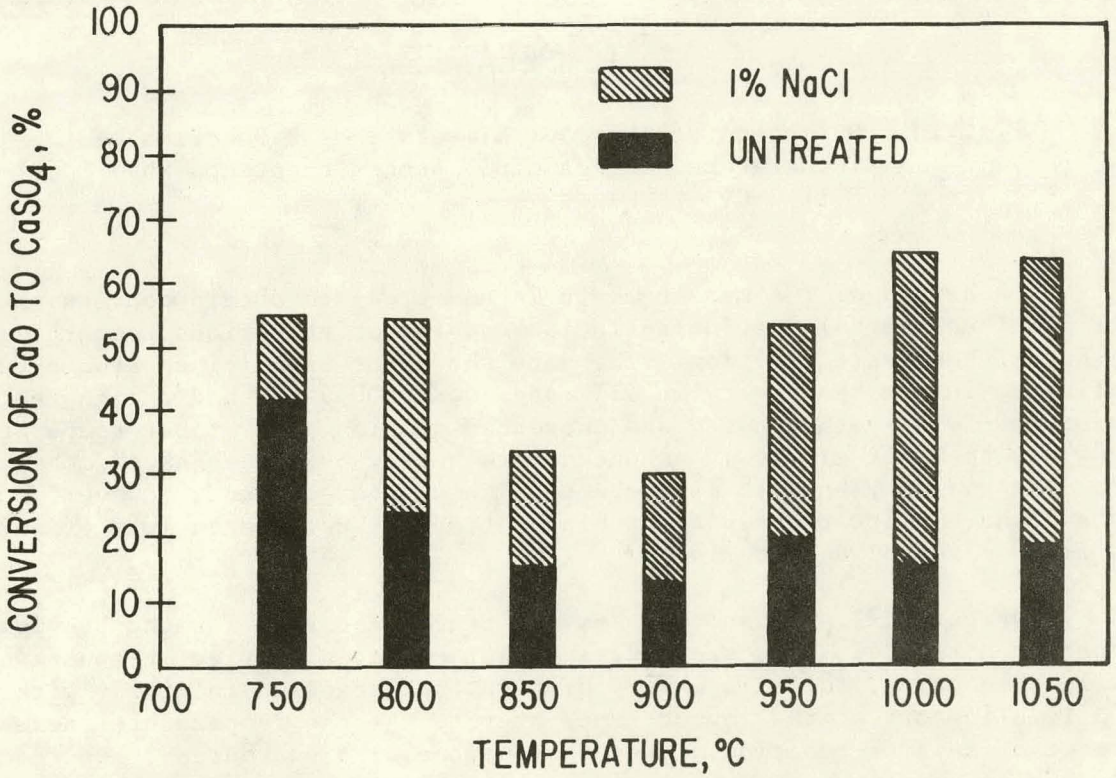

Fig. 19. Sulfation of ANL-9501 Limestone as a Function of Temperature. Precalcined stones treated with 1% NaCl (5 h)

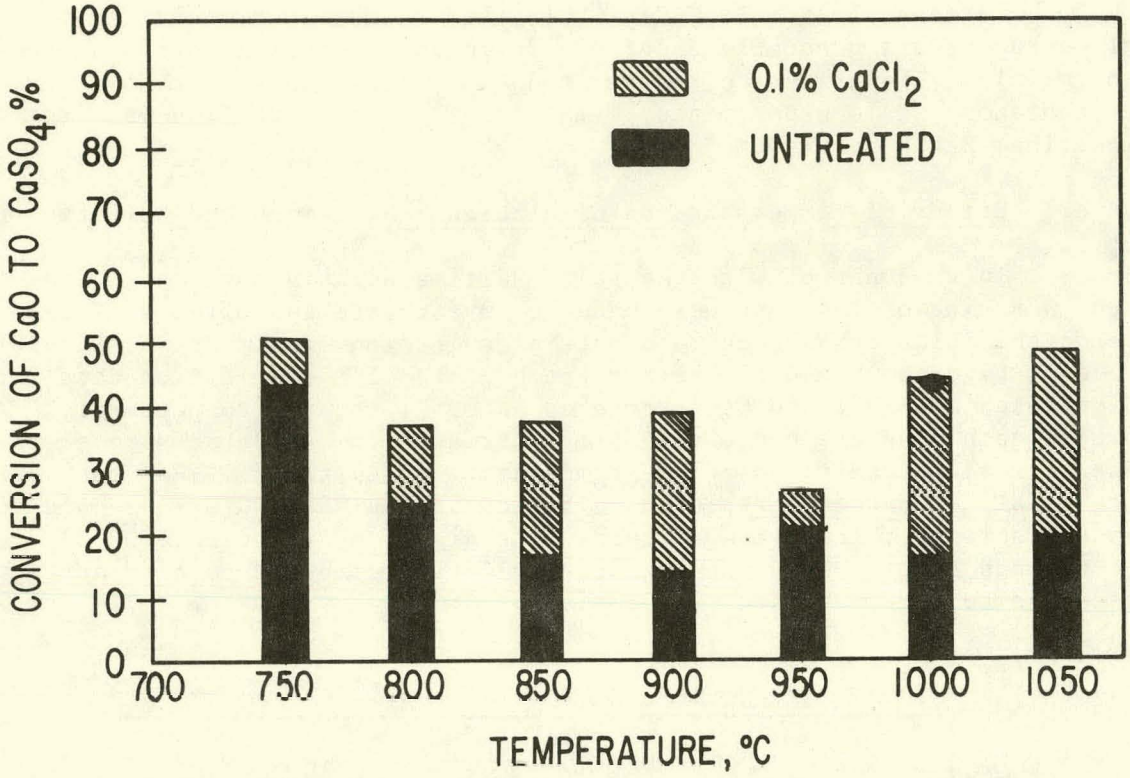

Fig. 20. Sulfation of ANL-9501 Limestone as a Function of Temperature. Precalcined stones treated with 0.1% $CaCl_2$ (5 h)

A series of TGA measurements is under way to obtain conversion values under simultaneous calcination/sulfation conditions at various temperatures with and without salt addition. The data shown for precalcined stones exhibit a definite minimum reactivity in all cases near 800-950°C and a high reactivity at 750°C for both treated and untreated samples. At higher temperatures (≥1000°C), the salt effect is enhanced--presumably by the enhanced mobility of the phases when salt is present. The untreated stone, however, continues to have a low reactivity at higher temperatures due to loss of surface area from solid-solid sintering.

Figures 21, 22, and 23 show the reaction curves for the previous bar graphs for untreated, NaCl-treated, and $CaCl_2$-treated samples, respectively. In all three cases, there is a very high rate of reaction initially with a rapid leveling-off at the lowest temperatures. As the temperature increases, the rate of initial reaction decreases (surface area decreases), but reaction continues longer (increased pore size). At still higher temperatures when salts are present (both NaCl and $CaCl_2$), the reaction rate again increases and remains significant for a longer time due to the presence of large amounts of liquid. The untreated stone, however, remains at an initial high rate of reactivity that rapidly falls off with no further reaction, suggesting that only the immediately available surface is reacting. A more detailed discussion of these data will be made when comparisons can be made with results obtained under simultaneous reaction conditions.

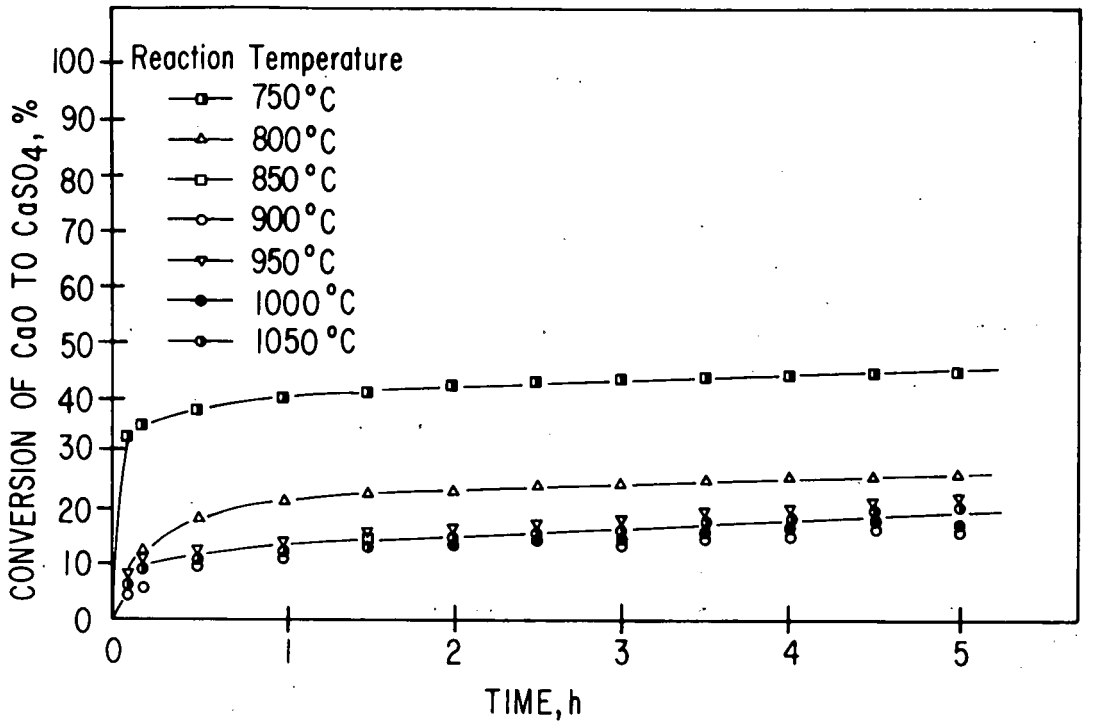

Fig. 21. Sulfation of ANL-9501 Limestone as a Function of Temperature in Precalcined Stones; Sulfation 0.3% SO_2, 5% O_2, 20% CO_2, and the Balance N_2

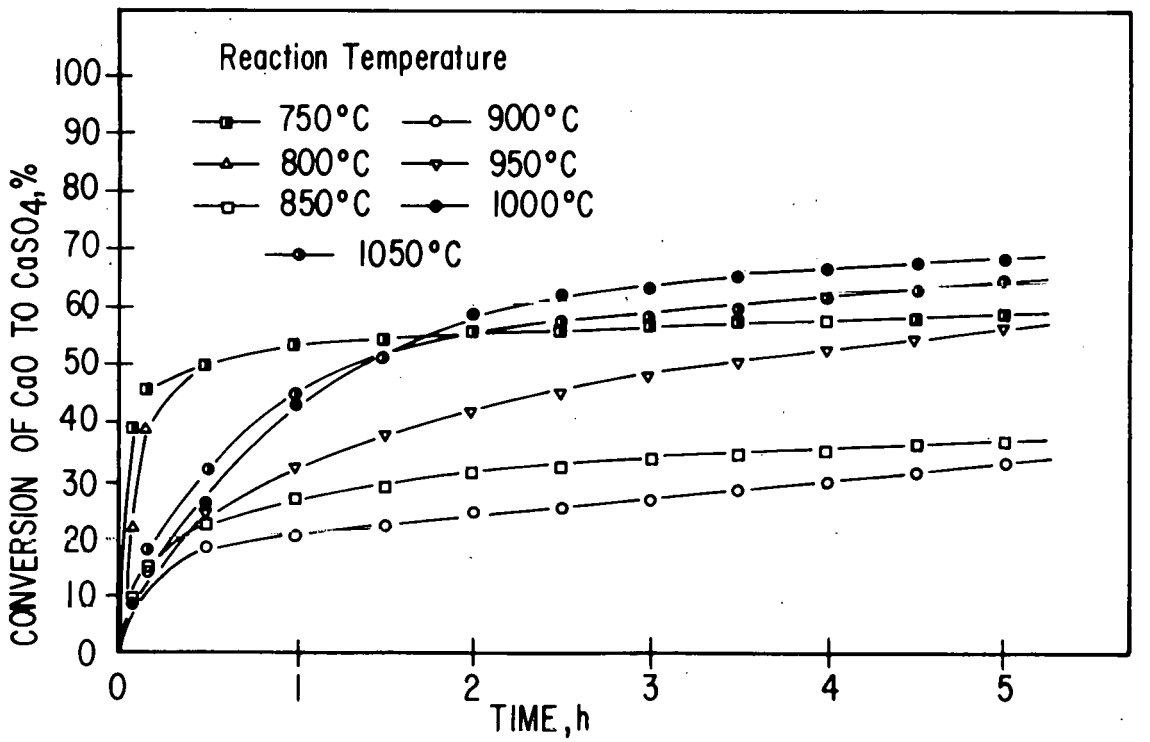

Fig. 22. Sulfation of 1359 Limestone as a Function of Temperature in Precalcined Stones Treated with 1% NaCl; Sulfation 0.3% SO_2, 5% O_2, 20% CO_2, and the Balance N_2

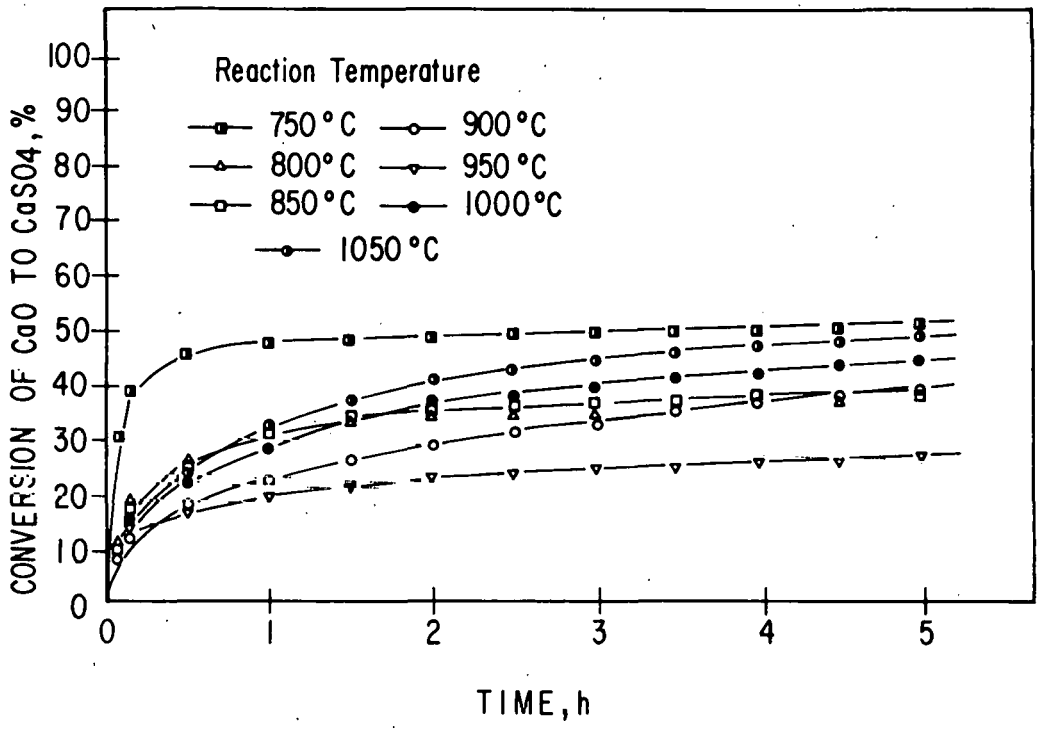

Fig. 23. Sulfation of ANL-9501 Limestone as a Function of Temperature in Precalcined Stones Treated with 0.1% $CaCl_2$; Sulfation 0.3% SO_2, 5% O_2, 20% CO_2, and the Balance N_2

Work to characterize coal combustor overflow samples and steady-state samples is continuing. This work will be extended to include laboratory simulation of combustor variables (such as water content and ash content) not considered previously.

The occurence of transient reducing conditions in the laboratory combustor as a possible source of sulfation enhancement will also be investigated. Duplication of combustor variables in a small quartz fluidized bed will be attempted in an effort to more clearly define conditions in a fluidized-bed coal combustor.

REFERENCES

1. D. L. Keairns et al., Fluidized Bed Combustion Process Evaluation, Environmental Protection Agency Report No. EPA-650/2-75-027-c (1975).

2. Pope, Evans, and Robbins, Inc., Multicell Fluidized-Bed Boiler Design, Construction, and Test Program, Combustion Systems Division, Monthly Progress Status Report No. 39 (December 1975).

Distribution for ANL/CEN/FE-79-5

Internal:

L. Burris
W. L. Buck
F. Cafasso
E. Carls
P. T. Cunningham
J. Fischer
H. Huang
B. R. Hubble
I. Johnson (20)
A. A. Jonke (30)
J. A. Kyger
R. V. Laney
S. Lawroski
S. H. Lee
J. F. Lenc
W. A. Ellingson
L. Cuba
G. M. Kesser
E. G. Pewitt
F. F. Nunes
W. Podolski
J. Royal
S. Siegel
J. W. Simmons
G. W. Smith
R. B. Snyder
W. M. Swift
F. G. Teats
S. Vogler
D. S. Moulton
D. S. Webster
W. I. Wilson
J. E. Young
R. Bane
E. J. Croke
J. D. Gabor
K. Jensen
N. Sather
J. Shearer
E. Smyk
C. B. Turner
A. B. Krisciunas
ANL Contract File
ANL Libraries (5)
TIS Files (6)

External:

DOE-TIC, for distribution per UC-90e (253)
Manager, Chicago Operations and Regional Office, DOE
Chief, Office of Patent Counsel, DOE-CORO
V. H. Hummel, DOE-CORO
President, Argonne Universities Association
Chemical Engineering Division Review Committee:
- C. B. Alcock, U. Toronto
- R. C. Axtmann, Princeton U.
- R. E. Balzhiser, Electric Power Research Inst.
- J. T. Banchero, U. Notre Dame
- T. Cole, Ford Motor Co.
- P. W. Gilles, U. Kansas
- R. I. Newman, Allied Chemical Corp.
- G. M. Rosenblatt, Pennsylvania State U.

D. H. Archer, Westinghouse Research Labs., Pittsburgh
E. C. Bailey, John Dolio and Associates, Chicago
S. Beall, Oak Ridge National Laboratory
O. L. Bennett, West Virginia U.
R. Bertrand, Exxon Research and Engineering, Linden, N. J. (5)
M. Boyle, Valley Forge Labs., Devon, Pa.
J. A. Brooks, Amoco Oil Co., Naperville, Ill.
R. D. Brooks, General Electric Co., Schenectady
C. Busch, Spectron Development Laboratory, Inc., Costa Mesa, Calif.
J. Chen, Lehigh U.
D. Cherrington, Exxon Research and Engineering Co., Florham Park, N. J.
J. Clark, Tennessee Valley Authority, Chattanooga
D. Clarke, Stearns-Roger, Denver
N. Coates, The MITRE Corp., McLean, Va.
R. C. Corey, Office of Fossil Energy Programs, USDOE
R. Covell, Combustion Engineering, Inc.
G. Curran, Conoco Coal Development Co., Library, Pa.
D. DeCoursin, Fluidyne Engineering Co., Minneapolis
J. Dodge, Tetra Tech, Inc., Arlington, Va.

M. Dudukovic, Washington U.
S. Ehrlich, Electric Power Research Inst.
M. Evans, Aerotherm Division of ACUREX Corp., Mountain View, Calif.
M. H. Farmer, Exxon Research and Engineering Co., Linden, N. J.
C. Fisher, U. Tennessee
T. Fitzgerald, Oregon State U.
J. F. Flagg, Universal Oil Products Co., Des Plaines, Ill.
H. B. Forbes, Stone & Webster Engineering Corp., Boston
F. Frable, Bethlehem Mines Corp.
R. L. Gamble, Foster Wheeler Energy Corp., Livingston, N. J.
D. E. Garrett, Garrett Energy Research and Engineering, Inc., Ojai, Calif.
L. Gasner, U. Maryland
J. Geffken, Office of Fossil Energy Programs, USDOE (5)
C. Georgakis, Massachusetts Inst. Technology
R. Glenn, Combustion Processes, Inc., New York City
J. S. Gordon, TRW, Inc., McLean, Va.
O. J. Hahn, U. Kentucky
W. Hansen, Babcock & Wilcox Co., Barberton, O.
M. J. Hargrove, Combustion Engineering, Inc.
R. D. Harvey, Illinois State Geological Survey, Urbana
R. Helfenstein, Illinois State Geological Survey, Urbana
R. G. Hickman, Lawrence Livermore Lab.
F. Hsing, Pratt & Whitney, East Hartford
D. Huber, Burns and Roe, Inc., Paramus, N. J.
F. D. Hutchinson, Gibbs and Hill, New York City
D. L. Keairns, Westinghouse Research Labs., Pittsburgh
C. B. Leffert, Wayne State U.
A. M. Leon, Dorr-Oliver, Inc., Stamford, Conn.
R. M. Lundberg, Commonwealth Edison Co., Chicago
J. J. Markowsky, American Electric Power Service Corp., New York City
M. J. Mayfield, Tennessee Valley Authority, Chattanooga
W. McCurdy, Office of Fossil Energy Programs, USDOE
J. Mesko, Pope, Evans and Robbins, New York City (2)
T. A. Milne, Solar Energy Research Inst.
W. G. Moore, Dow Chemical, USA, Midland, Mich.
S. Moskowitz, Curtiss-Wright Corp., Wood Ridge, N. J.
W. Norcross, Combustion Engineering, Inc.
T. A. Pearce, Dow Chemical, Freeport, Tex.
W. A. Peters, Massachusetts Inst. of Technology
C. Petty, Michigan State U.
M. I. Rednicki, Aerojet Energy Conversion, Sacramento
R. Reed, Pope, Evans and Robbins, Inc., Alexandria, Va.
A. F. Sarofim, Massachusetts Inst. Technology
S. Saxena, U. Illinois, Chicago
A. Sherman, Combustion Power Co., Menlo Park
C. Space, Reynolds, Smith & Hills, Jacksonville, Fla.
W. K. Stair, U. Tennessee
F. Staub, General Electric Corp., Schenectady
W. Steen, U. S. Environmental Protection Agency, Research Triangle Park (16)
M. Steinberg, Brookhaven National Lab.
W. Strieder, U. Notre Dame
S. E. Tung, Massachusetts Inst. Technology
V. Underkoffler, Gilbert Associates, Inc., Reading, Pa.
W. E. Wallace, Jr., Morgantown Energy Technology Center
F. A. Walton, Combustion Power Co., Menlo Park

A. E. Weller, Battelle Columbus Labs.
T. D. Wheelock, Iowa State U.
J. S. Wilson, Morgantown Energy Technology Center
K. Yeager, Electric Power Research Inst.
D. Zallen, Energy and Environmental Research Corp., Santa Ana
R. E. Zoellner, Stearns-Roger, Denver
J. F. Davidson, U. Cambridge, England
J. Highley, U. K. National Coal Board, Gloucestershire, England
H. R. Hoy, BCURA Ltd., Leatherhead, England
H. Schreckenberg, Bergbau-Forschung GmbH, Essen, Germany
G. Moss, Esso Research Centre, Abington, England
B. A. Wiechula, Imperial Oil Enterprises, Sarnia, Canada